Quaternary International 348 (2014) 247–265

Contents lists available at ScienceDirect

Quaternary International

journal homepage: www.elsevier.com/locate/quaint

The climate and vegetation of Marine Isotope Stage 11 – Model results and proxy-based reconstructions at global and regional scale

Thomas Kleinen [a,*], Steffi Hildebrandt [b], Matthias Prange [c], Rima Rachmayani [d], Stefanie Müller [b], Elena Bezrukova [e], Victor Brovkin [a], Pavel E. Tarasov [b]

[a] Max Planck Institute for Meteorology, Bundesstr. 53, 20146 Hamburg, Germany
[b] Freie Universität Berlin, Institute of Geological Sciences, Palaeontology, Malteserstraße 74-100, Building D, 12249 Berlin, Germany
[c] MARUM – Center for Marine Environmental Sciences and Faculty of Geosciences, University of Bremen, Klagenfurter Str., 28359 Bremen, Germany
[d] Faculty of Geosciences, University of Bremen, Klagenfurter Str., 28359 Bremen, Germany
[e] A.P. Vinogradov Institute of Geochemistry SB RAS, Favorskogo Str., Building 1A, Irkutsk, Russia

ARTICLE INFO

Article history:
Available online 14 January 2014

ABSTRACT

The climate of Marine Isotope Stage (MIS) 11, the interglacial roughly 400,000 years ago, is investigated for four time slices, 416, 410, 400, and 396 ka. We compare results from two climate models, the earth system model of intermediate complexity CLIMBER2-LPJ and the general circulation model CCSM3, to reconstructions of MIS 11 temperature, precipitation and vegetation, mainly from terrestrial records. The overall picture is that MIS 11 was a relatively warm interglacial in comparison to preindustrial, with Northern Hemisphere (NH) summer temperatures early in MIS 11 (416–410 ka) warmer than preindustrial, though winters were cooler. Later in MIS 11, especially around 400 ka, conditions were cooler in the NH summer, mainly in the high latitudes. Climate changes simulated by the models were mainly driven by insolation changes, with the exception of two local feedbacks that amplify climate changes. Here, the NH high latitudes, where reductions in sea ice cover lead to a winter warming early in MIS 11, as well as the tropics, where monsoon changes lead to stronger climate variations than one would expect on the basis of latitudinal mean insolation change alone, are especially prominent. Both models used in this study support a northward expansion of trees at the expense of grasses in the high northern latitudes early during MIS 11, especially in northern Asia and North America, in line with the available pollen-based reconstructions. With regard to temperature and precipitation changes, there is general agreement between models and reconstructions, but reconstructed precipitation changes are often larger than those simulated by the models. The very limited number of records of sufficiently high resolution and dating quality hinders detailed comparisons between models and reconstructions.

1. Introduction

Quantitative reconstructions of interglacial climates are of particular interests in light of the current anthropogenic warming, natural climate system dynamics (e.g. Solomon et al., 2007; Melles et al., 2012) and human–environment interactions (e.g. Yasuda and Shinde, 2004; Ruddiman, 2003; Weber et al., 2010). The temperature and moisture evolution for the most recent interglacial, the Holocene, has been established for different regions and selected time-slices using multi-decadal- to annual-resolution proxy records (e.g. Solomon et al., 2007; Wanner et al., 2008; Litt et al., 2009; Tarasov et al., 2009; Bartlein et al., 2011). For earlier interglacials, the availability of quantitative reconstructions remains relatively poor, and if reconstructions are available, the temporal and spatial resolution, as well as the dating quality of the climate archives, leave room for improvement.

The scientific interest in Marine Isotope Stage (MIS) 11 climate development has grown increasingly during the last decade (e.g. Burckle, 1993; Droxler et al., 2003; Rousseau, 2003; McManus et al., 2003; Desprat et al., 2005; Kandiano and Bauch, 2007; Ashton et al., 2008; Kariya et al., 2010). This interest is driven by the length of the MIS 11 interglacial, which at ~30 ka was longer than all subsequent interglacials, and the observed similarities to the current (MIS 1) interglacial in terms of orbital configuration, greenhouse gas concentrations, and sea level (e.g. Berger and Loutre, 1996; Hodell et al., 2000; Loutre and Berger, 2003; Lüthi et al., 2008; Tzedakis, 2010; Yin and Berger, 2010, 2012; McManus et al., 2011; Raymo and Mitrovica, 2012). Orbitally forced insolation variations and

* Corresponding author.
E-mail address: thomas.kleinen@mpimet.mpg.de (T. Kleinen).

1040-6182/$ – see front matter © 2014 Elsevier Ltd and INQUA. All rights reserved.
http://dx.doi.org/10.1016/j.quaint.2013.12.028

increased greenhouse gas concentrations have been proposed as the predominant forcings of higher temperatures, but during phases of muted precession and eccentricity the obliquity has also been proposed as the causal variable of interglacial length (Jouzel et al., 2007; Tzedakis et al., 2009). Model results by Yin and Berger (2012) indicate that the warmth of MIS 11 was due to its greenhouse gas concentration, while insolation alone would actually have led to a cooling.

While a substantial number of publications exist for proxy data representing MIS 11 climate and environments, surprisingly few studies using climate models and even fewer data-model comparisons have been published to date. Results obtained using a 2-dimensional climate model were presented by Loutre (2003) and Loutre and Berger (2003). Yin and Berger (2010, 2012) used the intermediate complexity model LOVECLIM to compare the climatic effects of changes in astronomical forcing and CO_2 on the climate of MIS 11 with other interglacials during the last 800,000 years. Herold et al. (2012) compared the climate of MIS 11 and several other interglacials (MIS 1, 5, 9, 11 and 19), using the full complexity climate model CCSM3. Melles et al. (2012) presented general circulation model (GCM) experiments with an interactive vegetation component (using GENESIS 3.0 coupled to BIOME4), focused on the Arctic region around Lake El'gygytgyn, NE Asia, for 410 ka, corresponding to the timing of peak northern hemisphere (NH) summer warmth. Finally, Milker et al. (2013) compared sea surface temperature (SST) reconstructions of MIS 11 with results from time slice simulations using CCSM3. In the current study we used one model of intermediate complexity (CLIMBER2-LPJ) and one comprehensive general circulation model (CCSM3) to simulate climate and vegetation dynamics during the earlier warmest part of MIS 11. We use CLIMBER2-LPJ for a transient simulation of MIS 11 climate, while using CCSM3 allows gaining a higher resolution insight into MIS 11 climate for selected time slices. Finally, climate changes determined by the two climate models are used to reconstruct the biome distribution, which is more often reconstructed than specific plants, by using the BIOME4 model.

A comparison of model simulations to climate and vegetation reconstructions based on proxy records helps in the evaluation of results and in better understanding the role of different climate drivers on past environments, from which both the data and modeling communities may profit. In this paper we present results of the model-simulated climate and vegetation cover during the MIS 11 full interglacial phase (~420–390 ka, roughly corresponding to substage 11.3 or 11c) – the earliest, longest and warmest phase of MIS 11 and one of the warmest interglacial intervals of the last 800 ka (Jouzel et al., 2007; Melles et al., 2012). These results are then compared and discussed together with published vegetation and climate reconstructions.

2. Data and methods

2.1. CLIMBER2-LPJ

CLIMBER2-LPJ (Kleinen et al., 2010) is a coupled climate carbon cycle model consisting of the earth model of intermediate complexity (EMIC) CLIMBER2 (Petoukhov et al., 2000; Ganopolski et al., 2001) coupled to the dynamic global vegetation model (DGVM) LPJ (Sitch et al., 2003; Gerten et al., 2004). This combination allows model experiments on time scales of an entire interglacial with land surface processes much more highly resolved (Kleinen et al., 2011).

CLIMBER2 consists of a 2.5-dimensional statistical-dynamical atmosphere with a latitudinal resolution of 10°. In the longitudinal direction the model resolves seven unevenly spaced sectors of subcontinental scale, which is equivalent to a mean longitudinal resolution of roughly 51°. It also contains an ocean model resolving three zonally averaged ocean basins with a latitudinal resolution of 2.5°, a sea ice model, and the dynamic terrestrial vegetation model VECODE (Brovkin et al., 2002). In addition, CLIMBER2 contains an oceanic biogeochemistry model, a model for marine biota (Ganopolski et al., 1998; Brovkin et al., 2002, 2007), and a weathering model.

To CLIMBER2 we have coupled the DGVM LPJ in order to investigate land surface processes at a significantly higher resolution. LPJ is run on a $0.5 \times 0.5°$ grid and is called at the end of every model year simulated by CLIMBER2. Monthly anomalies from the climatology of the temperature, precipitation, and cloudiness fields are passed to LPJ, where they are added to background climate patterns based on the Climatic Research Unit CRU-TS climate data set (New et al., 2000). In order to retain realistic interannual variability in these climate fields, the anomalies are not added to the climatology, but rather to the climate data for one year randomly drawn from the range 1901–1930. The change in the LPJ carbon pools is then passed back to CLIMBER2 as the carbon flux between atmosphere and land surface and is employed to determine the atmospheric CO_2 concentration for the next model year.

2.2. Community Climate System Model Version 3 (CCSM3)

The National Center for Atmospheric Research (NCAR) CCSM3 is a state-of-the-art coupled GCM that runs without any flux corrections. The global model is composed of four separate components representing atmosphere, ocean, land, and sea ice (Collins et al., 2006). Here, we use the low-resolution version of CCSM3 which is described in detail by Yeager et al. (2006). In this version, the resolution of the atmosphere is given by T31 (3.75° transform grid) spectral truncation with 26 layers, while the ocean model has a nominal horizontal resolution of 3° (like the sea-ice component) with 25 levels in the vertical. The latitudinal resolution of the ocean grid is variable, with finer resolution around the equator (0.9°). The land model is defined on the same horizontal grid as the atmosphere and includes components for biogeophysics, biogeochemistry, the hydrological cycle, as well as a dynamic global vegetation model. In order to improve the simulation of land hydrology, the Oleson et al. (2008) parameterizations for canopy interception and soil evaporation have been implemented for the land component.

2.3. BIOME4

Both CLIMBER2-LPJ and CCSM3 contain internal dynamic vegetation components. For the purpose of comparison to palaeovegetation reconstructions, the output of these models is less than ideal, though. DGVMs determine the grid cell coverage of certain plant functional types, but palaeovegetation reconstructions are usually reported in terms of biomes. We therefore also used the model BIOME4 to determine the biome distribution for the four selected time slices.

BIOME4 is a coupled carbon and water flux model that predicts the steady-state vegetation distribution, structure, and biogeochemistry, taking into account interactions between these effects (Kaplan, 2001). The model is the latest generation of the BIOME series of global vegetation models, which have been applied to a wide range of problems in biogeography, biogeochemistry and climate dynamics (Prentice et al., 1992; VEMAP Members, 1995; Haxeltine and Prentice, 1996; Jolly and Haxeltine, 1997; Kaplan et al., 2006; Tarasov et al., 2012). BIOME4 has been specifically developed with the intention of improving the simulation of cold-climate, high-latitude vegetation (Kaplan, 2001; Kaplan and New, 2006).

To identify the biome for a given grid cell, the model determines the plant functional types (PFT) that can grow in a particular grid cell from bioclimatic conditions, which include net primary production (NPP), leaf area index (LAI), mean annual soil moisture, and an index of vulnerability to fire. It then ranks the tree and non-tree PFTs that were determined, leading to an assignment to one of 27 global biomes.

2.4. Model experiments

We performed experiments with the two climate models described above, taking into consideration the characteristic features of MIS 11.3 (Fig. 1), including solar insolation and measured greenhouse gas concentrations. We undertook a transient experiment with CLIMBER2-LPJ from 420 ka to 390 ka, covering most of the full interglacial phase of MIS 11.3, driven by astronomical forcing (Berger, 1978) only. In order to get more detailed insight into spatial patterns of this interglacial, we also performed experiments with CCSM3 at four characteristic time slices within MIS 11.3 (Fig. 1). Experiments with CCSM3 cover roughly the precession minimum and maximum at 410 ka and 400 ka, respectively, which also are the 60°N June insolation maximum and minimum, and the obliquity maximum (416 ka) and minimum (394 ka), as indicated in Fig. 1. The precession is nearly identical for the latter two time slices.

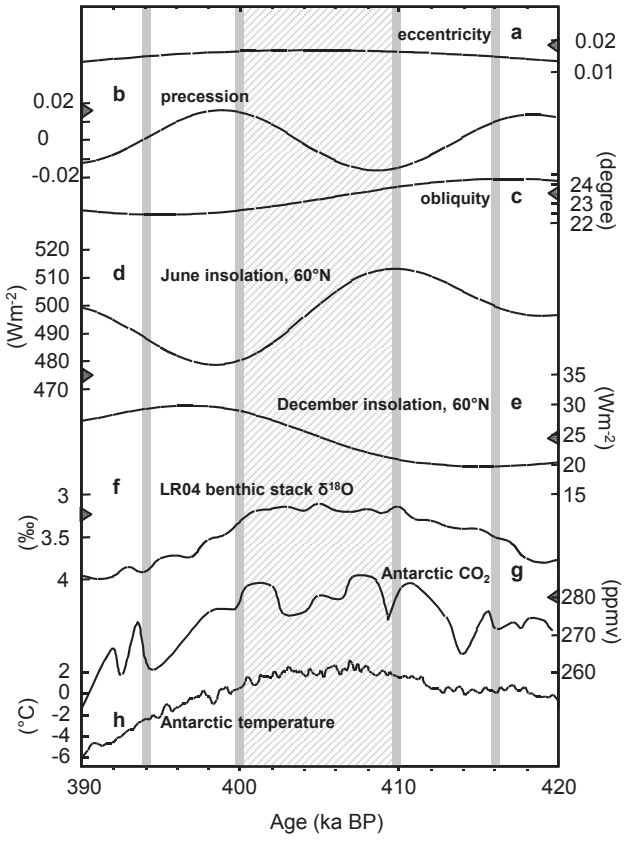

Fig. 1. Variations in Earth's orbital parameters: (a) eccentricity, (b) precession and (c) obliquity; (d) June and (e) December insolation at 60°N (Berger and Loutre, 1991); (f) global $\delta^{18}O$ stack (Liesicki and Raymo, 2005); (g) Antarctic CO_2 (Lüthi et al., 2008) and (h) temperature changes (Jouzel et al., 2007) during a selected time interval from 420 to 390 ka, which broadly corresponds to the warmest phase of MIS 11. Vertical grey bars indicate four time-slices analyzed by CLIMBER2-LPJ and CCSM3 models and discussed in this study; shaded area corresponds to the plateau in marine isotope (f) and Antarctic temperature record (h), indicating interglacial climatic optimum. Triangles at the vertical axes mark modern (preindustrial) values of the corresponding variable.

We initialised CLIMBER2-LPJ with corresponding orbital conditions and an atmospheric CO_2 concentration of 270 ppm, as shown by the EPICA Dome C ice core for 420 ka. The oceanic carbon cycle was initialised to out-of-equilibrium conditions as described in Kleinen et al. (2010), but appropriate for the conditions at 420 ka. The land carbon cycle was spun up for 2000 years under 420 ka boundary conditions and evolved freely thereafter. Atmospheric CO_2 was then determined interactively, with calculated CO_2 generally similar to reconstructed CO_2 from EPICA Dome C (Lüthi et al., 2008), as shown in Table 1. All other forcings are kept at preindustrial conditions. CLIMBER2-simulated CO_2 concentrations are listed in Table 1 for the four time slices. From this experiment we show results as 100 year mean values for the four time slices, with statistically insignificant areas masked. Statistical significance is determined using a *t*-test at 5% significance level.

Table 1
Greenhouse gas concentrations used in the experiments (Siegenthaler et al., 2005; Loulergue et al., 2008; Schilt et al., 2010), as well as CO_2 concentration modeled by CLIMBER2.

Experiments	CO_2 (ppmv)	CH_4 (ppbv)	N_2O (ppbv)	CLIMBER CO_2
0 ka BP	280	760	270	280
394 ka BP	275	550	275	276
400 ka BP	283	610	286	279
410 ka BP	284	710	282	280
416 ka BP	275	620	270	274

With CCSM3 a preindustrial control run was performed following the protocol established by the Paleoclimate Modeling Intercomparison Project, Phase 2 (PMIP-2) with respect to the forcing (Otto-Bliesner et al., 2006; Braconnot et al., 2007; Merkel et al., 2010). The control run was integrated for 600 years starting from present day initial conditions. For the selected time slices of MIS 11.3, appropriate orbital parameters (Berger, 1978) and greenhouse gas concentrations were prescribed as given in Table 1 (also Milker et al., 2013), while all other forcings (ice sheet configuration, ozone distribution, sulfate aerosols, carbonaceous aerosols, solar constant) were kept at preindustrial conditions. Starting from the last year of the (quasi)equilibrated preindustrial control run, all MIS 11.3 simulations were integrated for 400 years so that the surface climatologies could reach a statistical equilibrium. For each experiment, the mean of the last 100 simulation years was used for analysis. Statistical significance is determined using a *t*-test at 5% significance level, and areas where changes are not significant are masked.

For a direct comparison of CLIMBER2-LPJ and CCSM3 results in terms of simulated global biogeography on a 0.5 × 0.5° grid, we applied CCSM3-simulated climate changes to drive the LPJ model for the four selected time slices. Here, a 2000 year spinup was performed under constant boundary conditions according to the time slice investigated, followed by a 30 year experiment.

The climate changes determined with both models for the time slices were finally used to drive the BIOME4 model in order to simulate the main vegetation type (biome) distribution at 416, 410, 400 and 394 ka. The modern (preindustrial) biome distribution was simulated using an early twentieth-century climatology.

2.5. Proxy-based climate and vegetation reconstructions

For the purpose of this study we searched for proxy-based climate reconstructions of MIS 11.3 published elsewhere. We reviewed a total of 162 publications affiliated with MIS 11. However, this extensive search revealed that the majority of the publications

we reviewed provide qualitative, discontinuous and/or poorly dated information about the past climate only, while reliably dated quantitative reconstructions of temperature and precipitation are scarce. In the current paper we focus on a set of recently published continuous records of the MIS 11.3 interglacial climate and vegetation with well constrained chronologies, which are most suitable for a robust data-model comparison. Details of the palaeoclimate records and reconstruction methods are explained in the original publications and therefore are not presented here.

3. Model results

3.1. Temperature changes

We examine a set of four time slices during MIS 11.3. Since greenhouse gas concentrations, as listed in Table 1, are rather similar for all time slices, the main difference in boundary conditions are the different orbital configurations. Eccentricity is very low during all of MIS 11.3, leading to generally lower annual mean insolation than at present. The obliquity determines the latitudinal distribution of radiation, with high values implying higher insolation in the high latitudes, and precession influencing the seasonal distribution of radiation. Overall, the temperature changes modeled for the time slices very much reflect the orbital configuration present at the time.

At 416 ka, the obliquity maximum accompanied by moderately high NH summer insolation (Fig. 1d) and by low winter insolation (Fig. 1e), JJA (June, July, August) temperatures were generally warmer than preindustrial. CLIMBER2-LPJ shows a warming of 1–3 °C over the NH continents (Fig. 2a), while conditions over the Southern Hemisphere (SH) were mostly similar to modern (preindustrial). Africa between 10 and 20°N cools slightly, as does northern India, due to an enhanced monsoon. The stronger monsoon leads to enhanced cloudiness, i.e., an albedo increase, as well as evaporative cooling of the land surface due to the greater availability of moisture. Finally, enhanced tree coverage in these areas also leads to an increase in transpiration, leading to a further cooling. The JJA temperature change in the CCSM3 simulation (Fig. 2e) was similar in the NH extratropics, though it shows a slight cooling in some places of the SH, where CLIMBER2-LPJ shows temperatures similar to preindustrial. In both models the strongest JJA warming occurs over Asia and North America. For the NH winter (DJF; December, January, February) (Fig. 3a and e) both models show a slight cooling. This general cooling is more pronounced in CCSM3 (Fig. 3e), with maximum cooling reaching 2.5 °C in Asia, while CLIMBER2-LPJ (Fig. 3a) only cools by up to 1.4 °C. The exception to this pattern is the Arctic Ocean region, where a warming of roughly 2 °C over most areas of the Arctic Ocean is simulated by both models, with a maximum warming of 3 °C simulated by CLIMBER2-LPJ north of Siberia. This warming of the Arctic Ocean was also described by Yin and Berger (2012), as well as Herold et al. (2012). Sea ice coverage over the Arctic Ocean is substantially reduced, as shown in Fig. 4a and e. This reduced ice coverage leads to enhanced exchange of heat between ocean and atmosphere. In addition, there is the "summer remnant effect" (Yin and Berger, 2012) where enhanced JJA insolation warms the ocean surface layers leading to a reduction in sea-ice formation in the following winter.

At 410 ka, the precession minimum (NH summer insolation maximum), JJA temperatures were substantially warmer than preindustrial (Fig. 2b and f). The NH continents were warmer by 2–4.5 °C, the SH continents by 1–2 °C, and the oceans by 0–1.5 °C. The exceptions to this warming pattern are the monsoon regions in Africa and India. The general picture is rather similar in both models, though CCSM3 (Fig. 2f) shows strong warming in the Southern Ocean, less warming over other ocean areas and a stronger cooling in the African monsoon region. In the NH, the general JJA warming was accompanied by a winter cooling. As shown in Fig. 3b, CLIMBER2-LPJ-simulated DJF temperatures were cooler by 0.5–1.5 °C over the continents, and CCSM3 showed cooling by up to 4 °C in eastern Asia (Fig. 3f), while temperatures over the oceans were only slightly cooler or as warm as preindustrial (Fig. 3b and f). The NH polar latitudes warm substantially, by up to 4 °C due to the sea ice feedback and summer remnant effect.

At 400 ka, the precession maximum (NH summer insolation minimum), JJA temperatures over the NH continents north of 40°N were reduced by 0.5–1.5 °C, with CCSM3 showing a cooling by up to 4 °C in continental locations. The tropics, as well as the SH, show little temperature change in comparison to preindustrial (Fig. 2c and g). DJF temperatures over the NH continents were 0.5–1.5 °C warmer than preindustrial where significant (Fig. 3c and g), while the Arctic region was colder by 0.5–2 °C. This cooling may have been enhanced by the summer remnant effect, with sea ice coverage slightly enhanced (Fig. 4c and g). Climate change patterns are similar between the two models, with the exception of a warming in the North Atlantic/Nordic seas simulated by CCSM3 (Fig. 3g), also seen by Herold et al. (2012) and attributed to warmer throughflow to the Nordic seas.

At 394 ka, the obliquity minimum, JJA warming was confined to the tropics. CLIMBER2-LPJ shows temperatures similar to preindustrial north of 50°N and warming of up to 1.5 °C in the tropics (Fig. 2d). CCSM3, on the other hand shows a cooling of up to 1.5 °C in the high northern latitudes (Fig. 2h), but the low latitudes are warmer than preindustrial. CCSM3 also shows warming of 1–2.5 °C over the SH continents, which is not as pronounced in CLIMBER2-LPJ, probably due to the low resolution of the model. During DJF, temperatures are similar to preindustrial or up to 1 °C cooler. The Arctic Ocean area is cooler by 1 °C in CLIMBER2-LPJ and by up to 3 °C in CCSM3 (Fig. 3d and h). CCSM3 also shows a slight warming in the Greenland, Iceland and Norwegian seas area, as well as northern Australia, which receives considerably less precipitation.

This time slice, together with the model results for 416 ka, illustrates the climatic effects of obliquity variations particularly clearly. At 416 ka and 394 ka, the maximum and minimum in obliquity, respectively, occur, while eccentricity and precession have very similar values. Accordingly, the high latitudes of the NH are relatively warm at 416 ka (Fig. 2a and e), while the tropics are relatively cool, while it is just the opposite at 394 ka (Fig. 2d and h).

Therefore there is a general pattern of temperatures to first order reflecting insolation variations, with warmer NH JJA temperatures simulated during the analyzed time slices with the exception of 400 ka. Similarly, NH DJF temperatures were somewhat cooler at most times, reflecting the low NH DJF insolation (Fig. 1e), though a slight warming can be seen at 400 ka. This general pattern is altered for regions, where strong regional effects modify the response. The Arctic areas are warmer than preindustrial at 416 and 410 ka in both models, despite the general winter cooling. Here, the magnitude of warming cannot be explained purely by insolation. Instead, significantly decreased sea ice coverage (Fig. 4) in combination with the summer remnant effect leads to enhanced heat exchange between atmosphere and ocean in the NH high latitudes, warming the very high latitudes. Similarly, changes in monsoon patterns, where monsoons are strengthened during times of high NH summer insolation, lead to a strong cooling in the monsoon regions where enhanced cloud coverage leads to an albedo increase while the additional moisture also leads to evaporative cooling. In general, the temperature change patterns determined by the two climate models were qualitatively similar, with CCSM3 reacting slightly more sensitively to insolation changes. CCSM3 also resolves considerably more regional details.

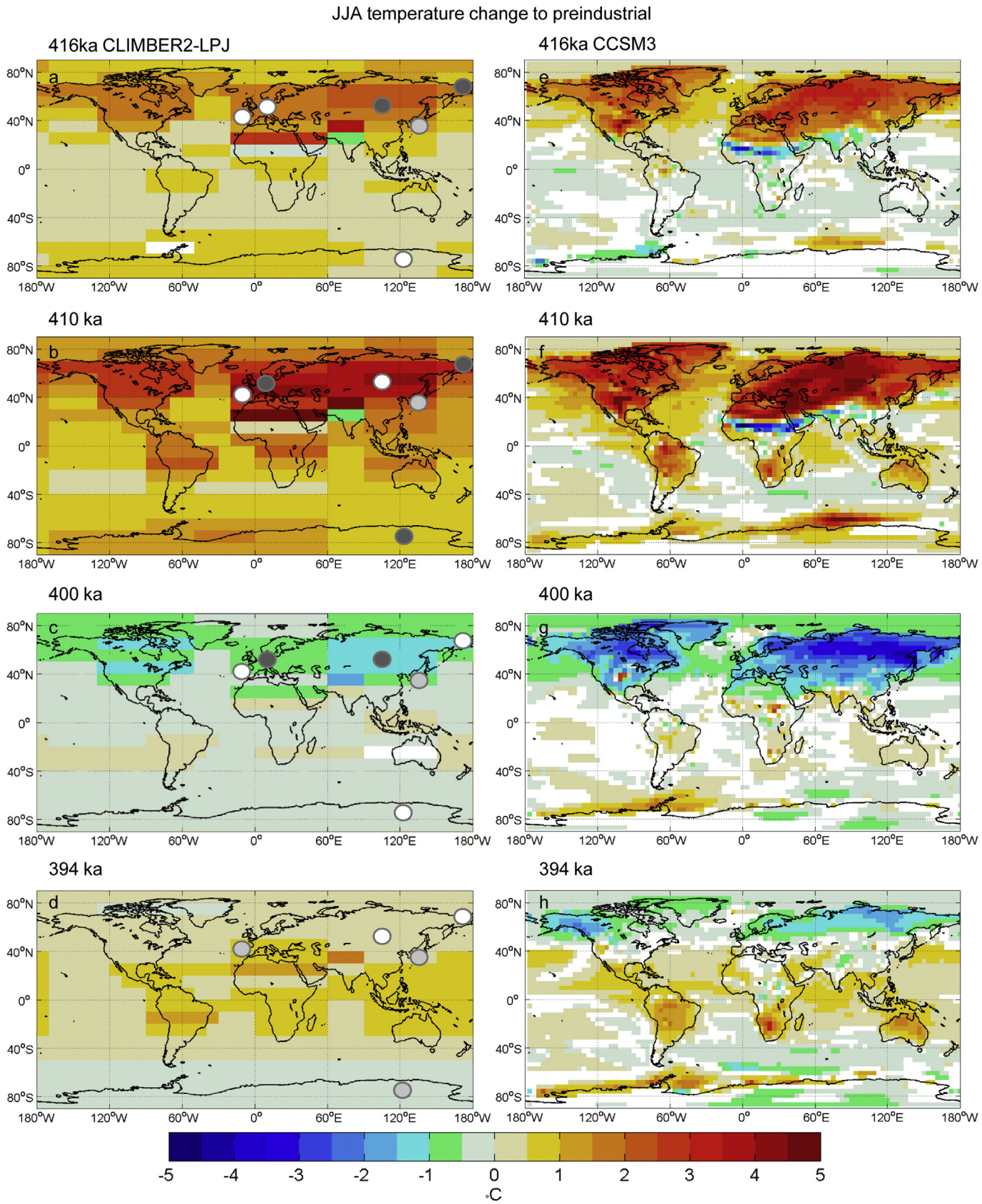

Fig. 2. Modeled changes in mean June–July–August surface temperature between 416 (a, e), 410 (b, f), 400 (c, g) and 394 ka (d, h) and preindustrial: (a–d) CLIMBER2-LPJ; (e–h) CCSM3. Areas with non-significant results are masked. Circles indicate qualitative proxy trend. White: no change, dark grey: increase, light grey: decrease.

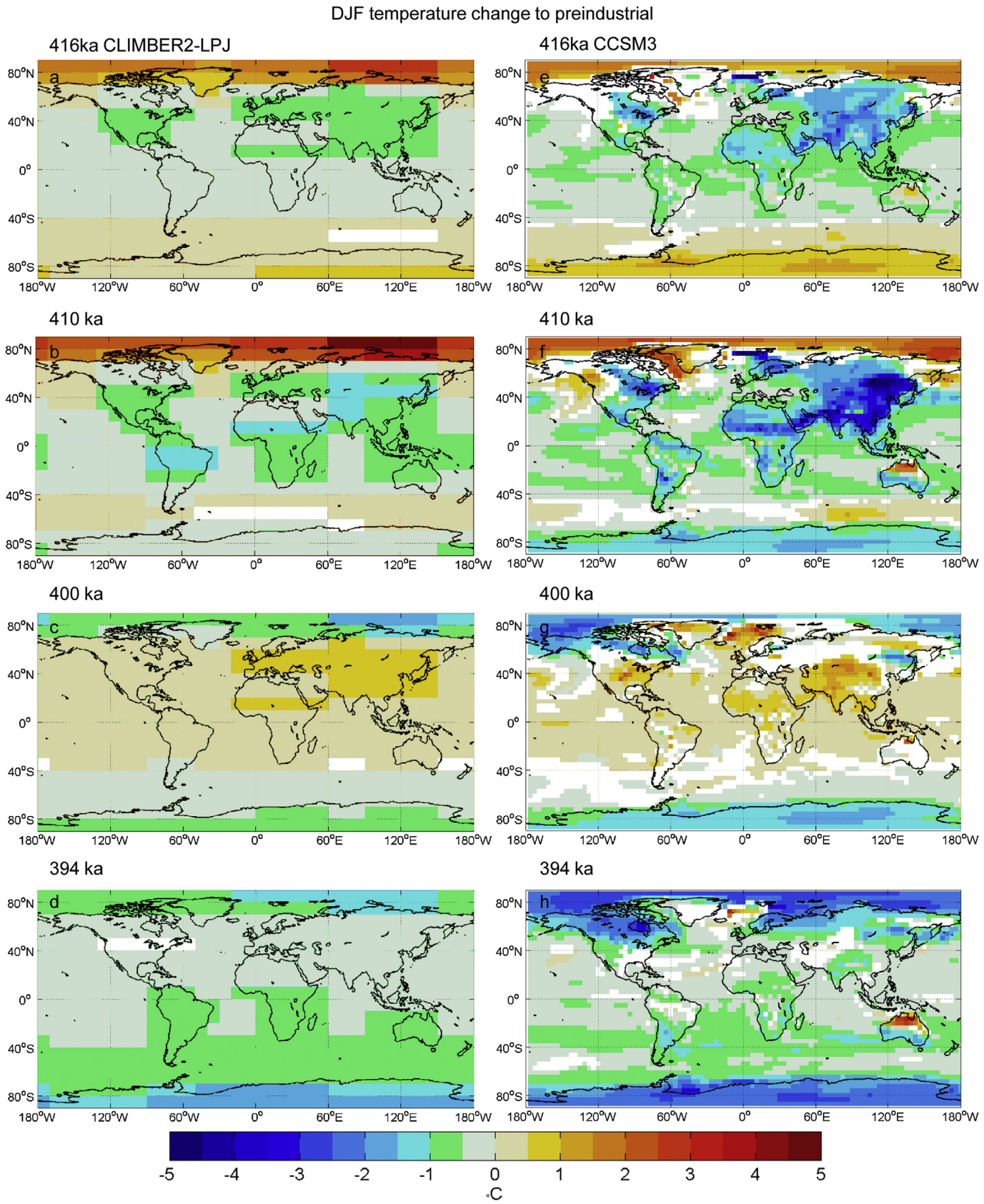

Fig. 3. Modeled changes in mean December-January-February surface temperature between 416 (a, e), 410 (b, f), 400 (c, g) and 394 ka (d, h) and preindustrial: (a–d) CLIMBER2-LPJ; (e–h) CCSM3. Areas with non-significant results are masked.

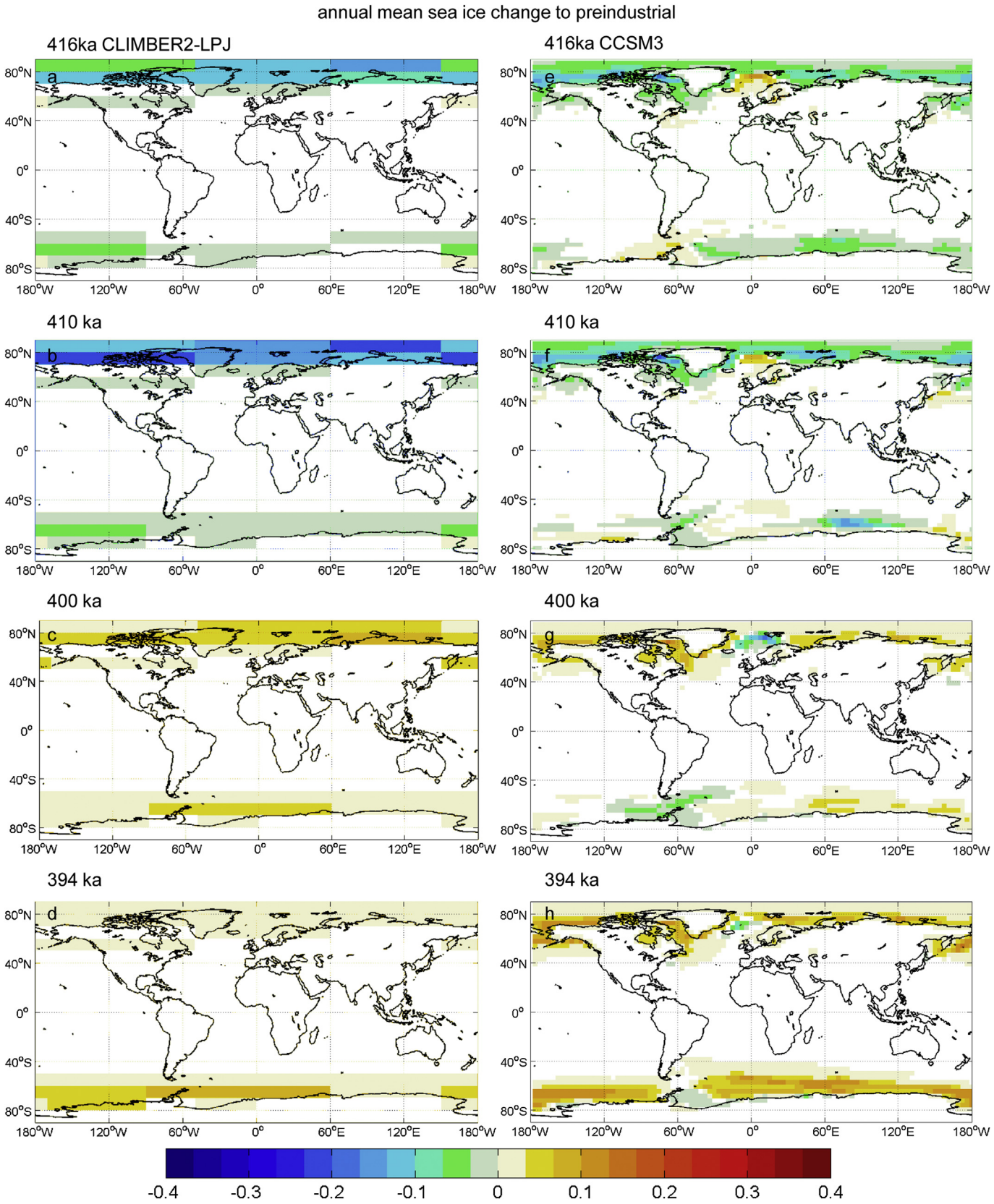

Fig. 4. Modeled changes in annual mean sea ice fraction between 416 (a, e), 410 (b, f), 400 (c, g) and 394 ka (d, h) and preindustrial: (a–d) CLIMBER2-LPJ; (e–h) CCSM3. Areas with non-significant results are masked.

3.2. Precipitation changes

The modeled changes in precipitation also reflect the orbital influence on climate through insolation, as well as monsoon changes. The tropical precipitation changes seen over the Atlantic and the eastern Pacific Ocean during all time slices, especially in CCSM3, reflect the movement of the intertropical convergence zone (ITCZ). To first order, increases in NH JJA insolation lead to a northward movement of the ITCZ, while decreases in NH insolation lead to a southward movement. Therefore precipitation decreases in the NH tropical Atlantic and eastern Pacific, while it increases in the SH tropics at 400 ka. This pattern is reversed for the other three time slices. This linear response to insolation changes is modified strongly for the monsoon regions in Africa and Asia including India, as well as North America. Generally, the monsoon systems are stronger for high NH summer insolation than for low values. Higher insolation leads to larger land-ocean temperature gradients driving the circulation since land warms more than the surrounding oceans (Fig. 2). Therefore, precipitation is stronger at 416 ka and 410 ka in North Africa, India, and Central America. For Eastern Asia there is a difference between CLIMBER2-LPJ and CCSM3. For CLIMBER2-LPJ there is a general increase in precipitation in eastern Asia, while CCSM3 shows a decrease in precipitation. This is supported by Herold et al. (2012), who have shown that CCSM3 simulates an inverse relationship between local insolation and East Asian monsoonal rainfall. CLIMBER2-LPJ generally shows very small changes in precipitation, with most areas less than 50 mm/a different from preindustrial. At 416 ka CLIMBER2-LPJ (Fig. 5a) shows changes in the monsoon regions. The African monsoon strengthens and precipitation increases by up to 400 mm/a between 10 and 30°N. Similarly, an enhanced Indian monsoon causes increases in precipitation by 300 mm/a in northern India. In CCSM3 (Fig. 5e) the changes in precipitation appear more variable spatially, as is to be expected in a model with a substantially higher resolution. Here, the northward shift of the ITCZ leads to increases in precipitation in the NH equatorial region and decreases in the SH tropics, though there is an increase in precipitation over the western Indian Ocean. The African monsoon strengthens as well, increasing precipitation over Africa, but the increase over India appears less pronounced than in CLIMBER2-LPJ. For 410 ka, CLIMBER2-LPJ (Fig. 5b) shows a slight increase in precipitation north of the equator, in the very high northern latitudes and in eastern Asia, but a strong increase in (sub-) tropical Africa and India. CCSM3 (Fig. 5f) displays substantially more spatial variability with precipitation increases in the NH tropical Atlantic and eastern Pacific, and decreases in the SH tropics. The Indian and African monsoons are strengthened, leading to precipitation increases in Africa, the Arabian peninsula and India. Precipitation strongly increases over the Indian Ocean, but decreases over the western Pacific, with precipitation in northern Australia decreasing considerably. Therefore we again see an overall northward shift of the ITCZ with changes in the monsoon systems modifying the otherwise meridional structure of precipitation changes.

At 400 ka, on the other hand (Fig. 5c and g), the general pattern of precipitation changes consists of increases in the SH tropics and western Pacific and decreases in the NH tropics, i.e., there is a southerly shift of the ITCZ, as well as a decrease in the monsoons. The amplitude of these changes is much smaller than for the other time slices, though. At 394 ka, finally, the patterns of precipitation change in CLIMBER2-LPJ (Fig. 5d) are similar to 416 ka. There is northerly shift of the ITCZ, as well as slight increases in the monsoons, with the exception of East Asia. In CCSM3, the Indian monsoon increase is slightly more pronounced, with precipitation rising by up to 150 mm/a (Fig. 5h).

The differences between the models are much more pronounced in the precipitation changes than in the temperature changes. Precipitation patterns are much more localized, for example along coastlines, than temperature patterns. Therefore the higher resolution of CCSM3, along with different parameterizations, leads to a considerably more refined precipitation field. While CLIMBER2-LPJ shows a similar general pattern of ITCZ and monsoon changes, these are at much smaller amplitude than the projections by CCSM3 and obviously with much less regional detail.

3.3. Vegetation changes

The modeled vegetation changes reflect the insolation-driven climate changes. At 416 ka, the LPJ model shows a northward shift of the northern tree line (Fig. 6a and e) relative to the preindustrial control simulation. This is slightly more pronounced using the climate changes determined by CCSM3. Similarly, steppe areas in Asia and North America expand, shifting the tree line there to the north. The Sahel area in Africa shows increases in tree cover, and the area covered by grass (not shown) moves even further to the north here. Very similar vegetation changes occur for 410 ka (Fig. 6b and f), though more pronounced, reflecting the larger climate changes. Tree cover also increases in the monsoon-influenced regions in India and eastern Asia, but the models disagree with respect to the exact locations due to the more localized precipitation changes in CCSM3.

These vegetation changes reflect the climatic changes. The northward shift of the northern tree line is driven by the lengthening of the growing season in the warmer climate, while the expansion of steppe areas is caused by drying due to enhanced evapotranspiration in combination with decreased precipitation. Similarly the changed tree coverage in the Sahel and the monsoon regions reflects the additional precipitation received by these areas. For 400 ka, shown in Fig. 6c and g, the models simulate the reverse: A southerly movement of the northern tree line, due to JJA cooling of the NH high latitudes leading to a shorter growing season, and an increase in tree cover in the mid-latitude steppe regions due to reduced evapotranspiration under cooler conditions. At 394 ka, finally, changes in tree cover are very small for CLIMBER2-LPJ (Fig. 6d), but CCSM3-LPJ (Fig. 6h) behaves differently. Here, the northern tree line shifts much further south, especially in eastern Siberia. This latter difference is due to the very different temperature change at 394 ka, where CLIMBER2-LPJ shows much weaker cooling than CCSM3.

Expressed in terms of biomes, as determined by the BIOME4 model, the picture is very similar. We show the biome distribution for preindustrial climate in Fig. 7. In comparison to this reference state, the climate changes at 416 ka lead to a northward shift of the taiga-tundra boundary, with the shift slightly more pronounced in CCSM3 (Fig. 8a and e). In central Asia, the mixed forest shown for preindustrial climate is replaced by grassland. In central Europe, some of the mixed forest is replaced by coniferous forest, especially in the Baltic region. In most other areas vegetation changes rather little.

For 410 ka, the climate from both models again leads to a northward move of the taiga-tundra boundary (Fig. 8b and f), further north than at 416 ka. In central Asia, the mixed forest and some of the taiga forest shown for preindustrial climate are replaced by grassland. In central Europe, cool mixed forest is replaced by temperate deciduous forest at the southern boundary of the range, with an eastward expansion of temperate deciduous forest shown by CCSM3. In CLIMBER2-LPJ, on the other hand, the mixed forest is replaced by temperate woodland in southern Europe. Deserts in Asia shrink in both models, and in CLIMBER2-LPJ much of the Sahara is turned into a shrubland. In most other areas

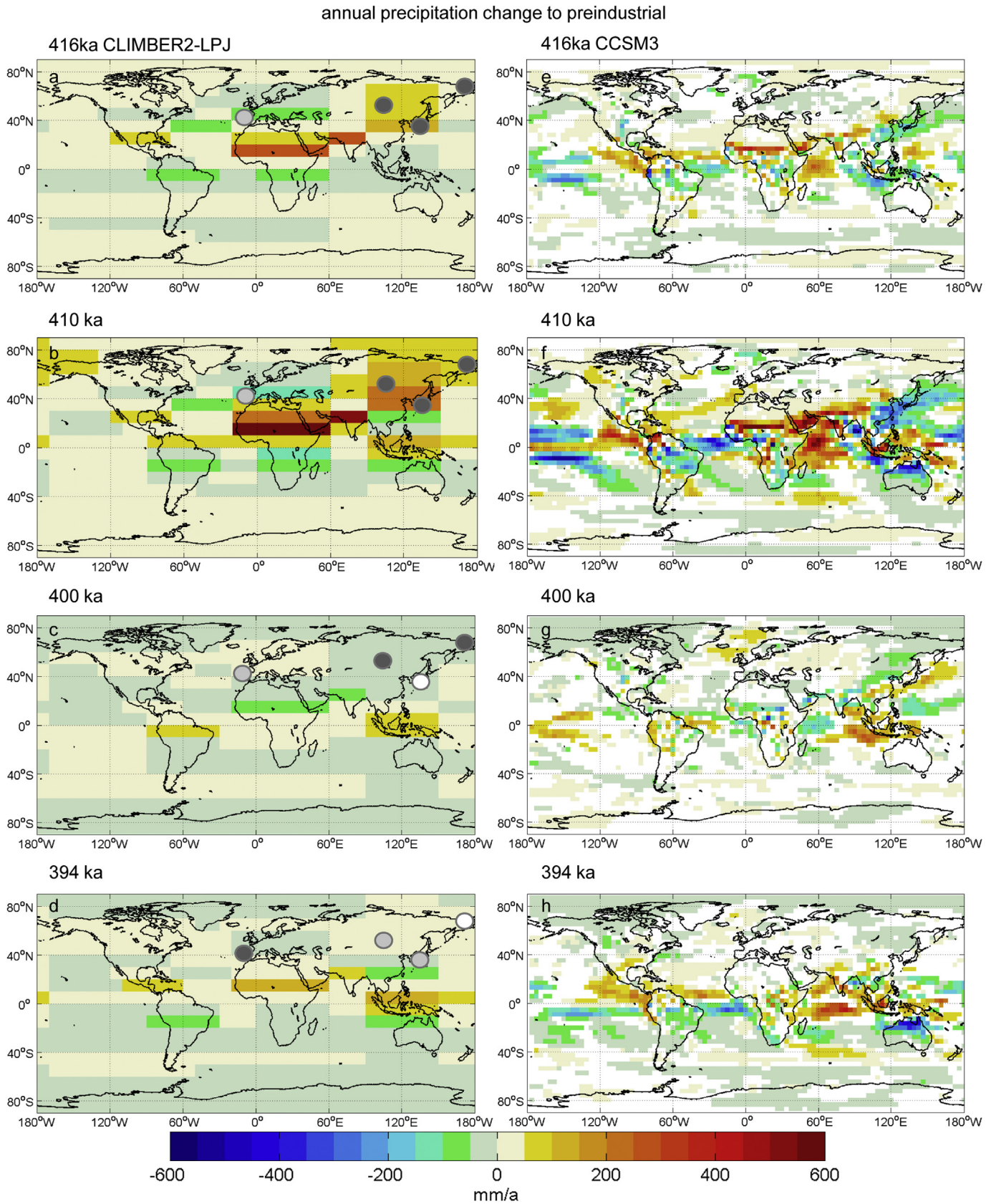

Fig. 5. Modeled changes in mean annual precipitation between 416 (a, e), 410 (b, f), 400 (c, g) and 394 ka (d, h) and preindustrial: (a–d) CLIMBER2-LPJ; (e–h) CCSM3. Areas with non-significant results are masked. Circles indicate qualitative proxy trend. White: no change, dark grey: increase, light grey: decrease.

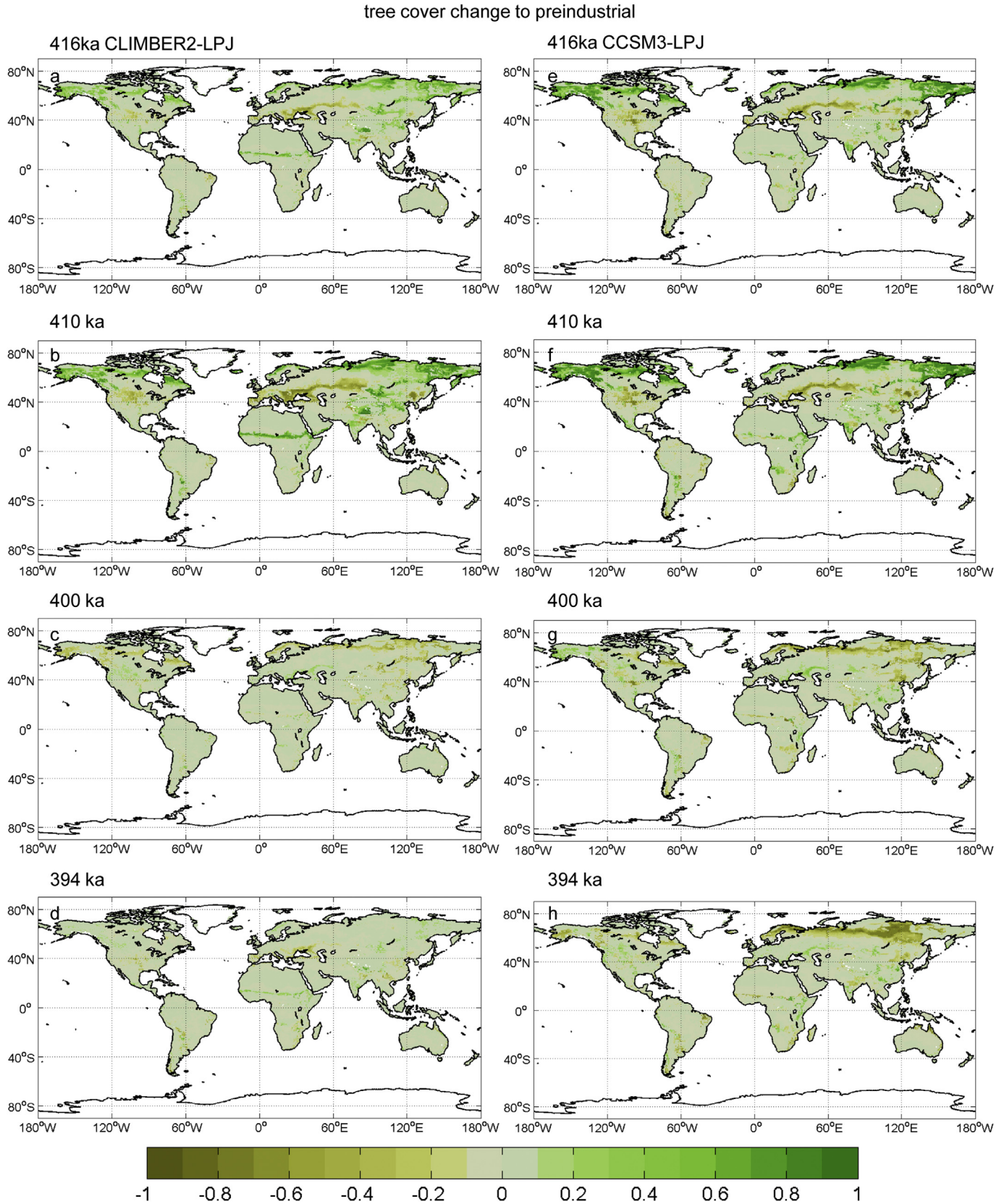

Fig. 6. Modeled changes in tree cover as grid cell fraction between 416 (a, e), 410 (b, f), 400 (c, g) and 394 ka (d, h) and preindustrial: (a–d) CLIMBER2-LPJ; (e–h) CCSM3-LPJ.

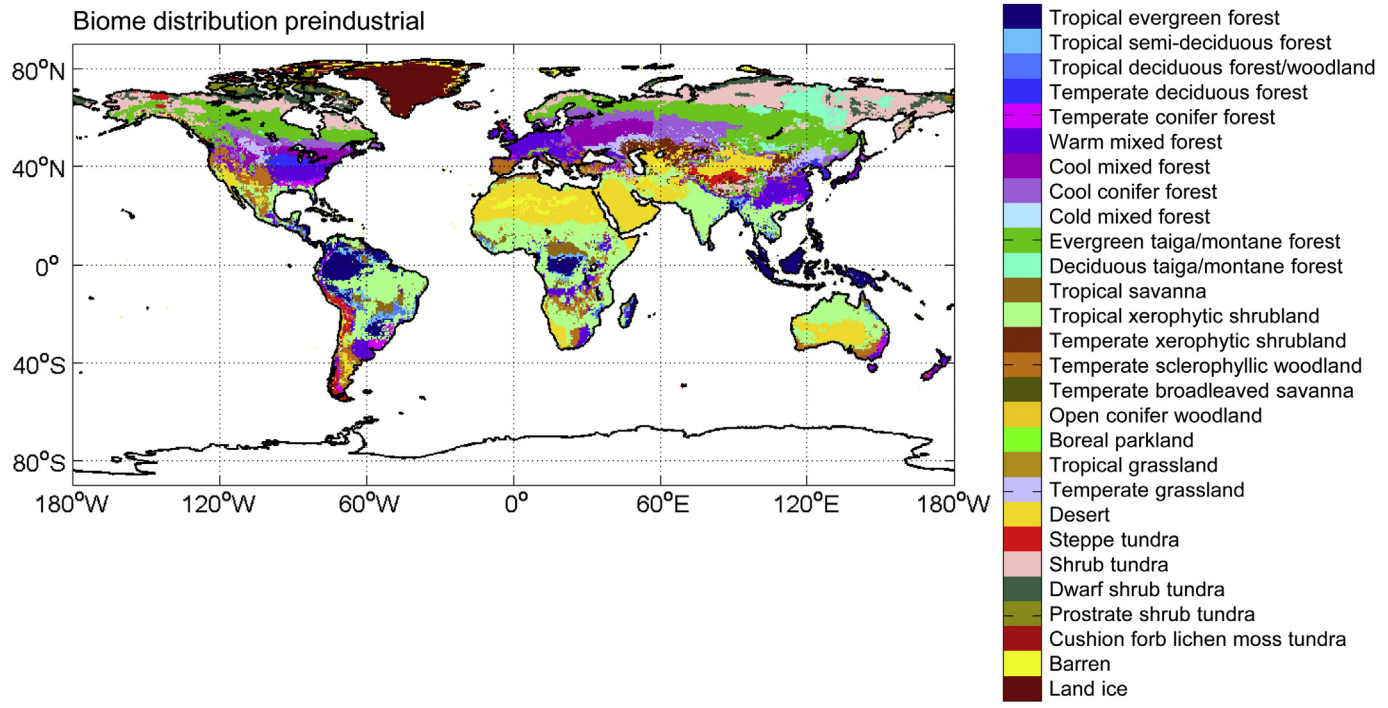

Fig. 7. Modeled biome distribution for preindustrial climate.

vegetation changes rather little. At 400 ka, biome changes in CLIMBER2-LPJ are very small, but in CCSM3 the taiga-tundra boundary shifts slightly southwards and the extent of deciduous and mixed forest declines in central Europe. For 394 ka (Fig. 8d and h), finally, the taiga-tundra boundary is shifted southwards, especially in eastern Siberia, and some cool mixed forest is replaced by coniferous forest in eastern Europe, as shown in both models, but more pronounced in CCSM3.

4. Discussion

The following discussion is focused on the similarities and differences in the MIS 11.3 climate and vegetation, which appear in the current model simulations and in the published proxy-based reconstructions. In this publication we mainly focus on terrestrial records, a summary of marine records for MIS 11.3 can be found in Milker et al. (2013).

4.1. Temperature changes

Some of the proxy records of MIS 11.3 from previously published studies consider it the longest and warmest interglacial of past 500 ka based on the study of marine isotopic records (Howard, 1997; Droxler et al., 1999; Melles et al., 2012). Other studies investigating marine and continental records, however, indicated that the evidence about the degree of warming during MIS 11.3 remained complex (Droxler and Farrell, 2000), with the temperature estimates varying from similar to the present to warmer than present from place to place (Rousseau, 2003). Both large uncertainties of the reconstruction methods and the lack of accurate chronologies for the sparsely available terrestrial records often preclude a reliable correlation between marine and terrestrial archives and complicate the comparison of geological data with model simulations (Desprat et al., 2005; Prokopenko et al., 2010).

Among the very few sites in the SH with MIS 11.3 climate data, the temperature records from Antarctic ice cores (i.e. Jouzel et al., 2007) are by far the best in terms of temporal resolution and dating quality. The EPICA Dome C reconstruction (Figs. 1h and 9i) demonstrates that the mean annual temperature was similar to the average of the last 1000 years at 416 ka and 400 ka, about 2 °C warmer at 410 ka, reaching up to +3 °C at 407 ka, but about 2 °C colder at 394 ka (Jouzel et al., 2007). Simulations with both models show similar trends, simulated Antarctic temperatures are slightly warmer than present at 416 ka, similar to present at 410 ka, but colder than present at 400 and 394 ka.

The NH continents reveal a number of sites available for a data-model comparison. Continuous pollen records from Asian lakes are one of the major terrestrial sources of information used to reconstruct regional climate variability during MIS 11.3. A sediment core from Lake El'gygytgyn (67.5°N, 172°E) in northeastern Siberia provides a continuous, high-resolution record from the Arctic, spanning the past 3.58 million years (Melles et al., 2012; Brigham-Grette et al., 2013). This record shows that the MIS 11.3 interval was one of the warmest and longest interglacials during the Quaternary, with mean temperatures of the warmest month (MTWM) being ~6 °C and 5 °C higher (Fig. 9a) than modern at 416 and 410 ka, respectively, in line with the model simulations. The reconstructed summer temperatures are similar to present day values at 400 and 394 ka, while colder temperatures appear in the CCSM3 simulations during both time slices and in the CLIMBER2-LPJ simulation at 400 ka. Melles et al. (2012) compared the reconstructed temperatures around Lake El'gygytgyn with GCM simulations using greenhouse gas and orbital forcing (Yin and Berger, 2010) at 409 ka and found that the peak summer warmth is difficult to explain with greenhouse gas and astronomical forcing alone. Results derived with an ice-free Greenland and the heat flux under Arctic Ocean sea ice increased by 8 W m^{-2} led to a simulated MTWM value which was closer to the reconstructed one, suggesting the importance of amplifying feedbacks and teleconnections (e.g. Yin and Berger, 2010; Melles et al., 2012). In our model simulations the decrease in sea ice area leads to a warming feedback amplifying the insolation-induced warming, supporting their results.

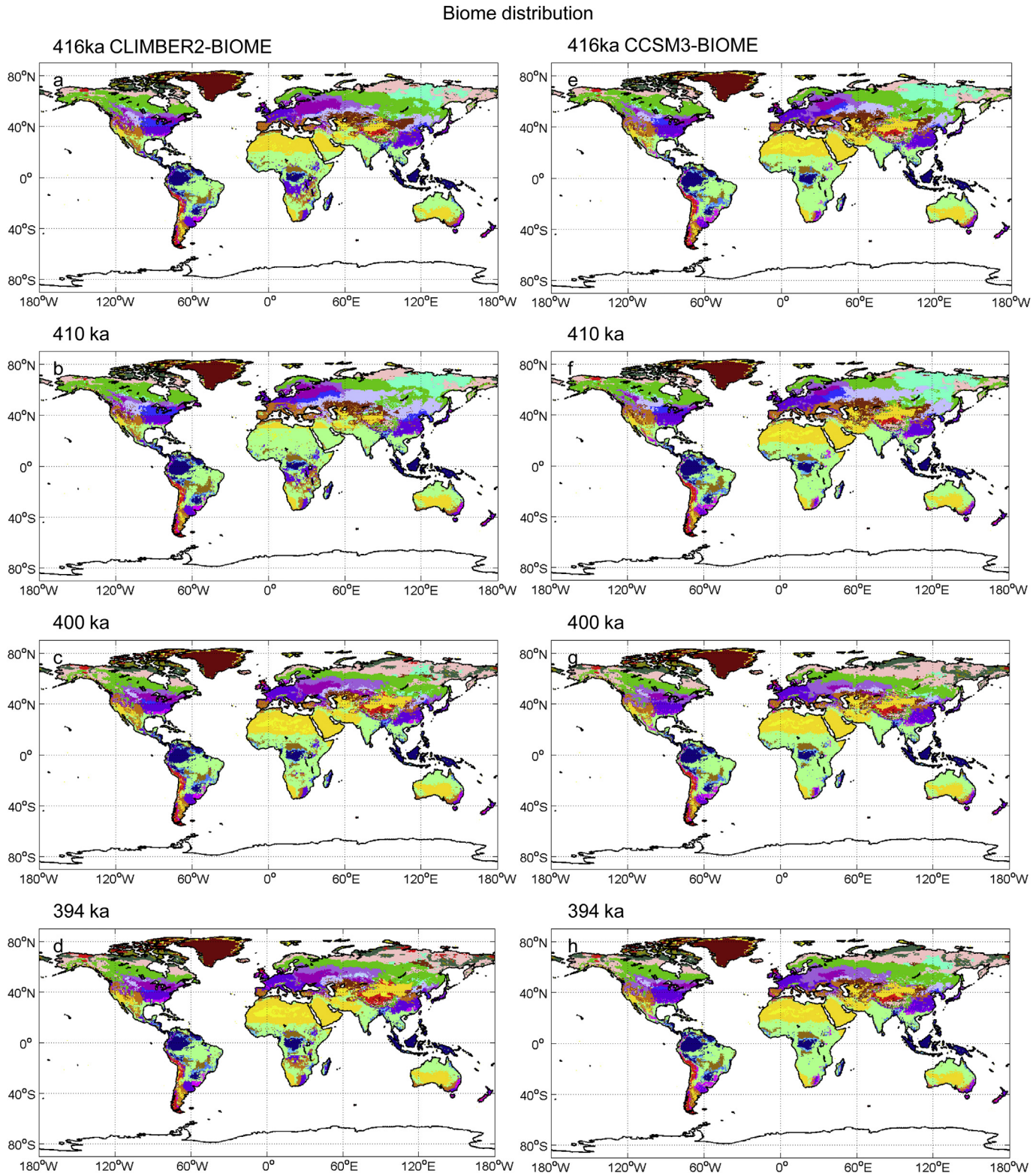

Fig. 8. Modeled biome distribution for 416, 410, 400 and 394 ka in CLIMBER2-LPJ (a–d) and in CCSM3 (e–h). Legend for the biome types as in Fig. 7.

A bioproductivity proxy (Prokopenko et al., 2006) and pollen records from Lake Baikal (Shichi et al., 2009) also suggest a very long and exceptionally warm interglacial during MIS 11.3. The pollen-based climate reconstruction derived from the core BDP-99 (52.09°N, 105.26°E) from Lake Baikal (Prokopenko et al., 2010) confirms these earlier conclusions. The reconstructed trends are similar to the results from Lake El'gygytgyn, but the increase in MTWM is more moderate, i.e., ca. 1–2 °C higher than the modern value (Fig. 9c). This amplitude is more comparable to the summer SST reconstructions from the sites U1313 (41.0°N, 32.96°W, Fig. 9e)

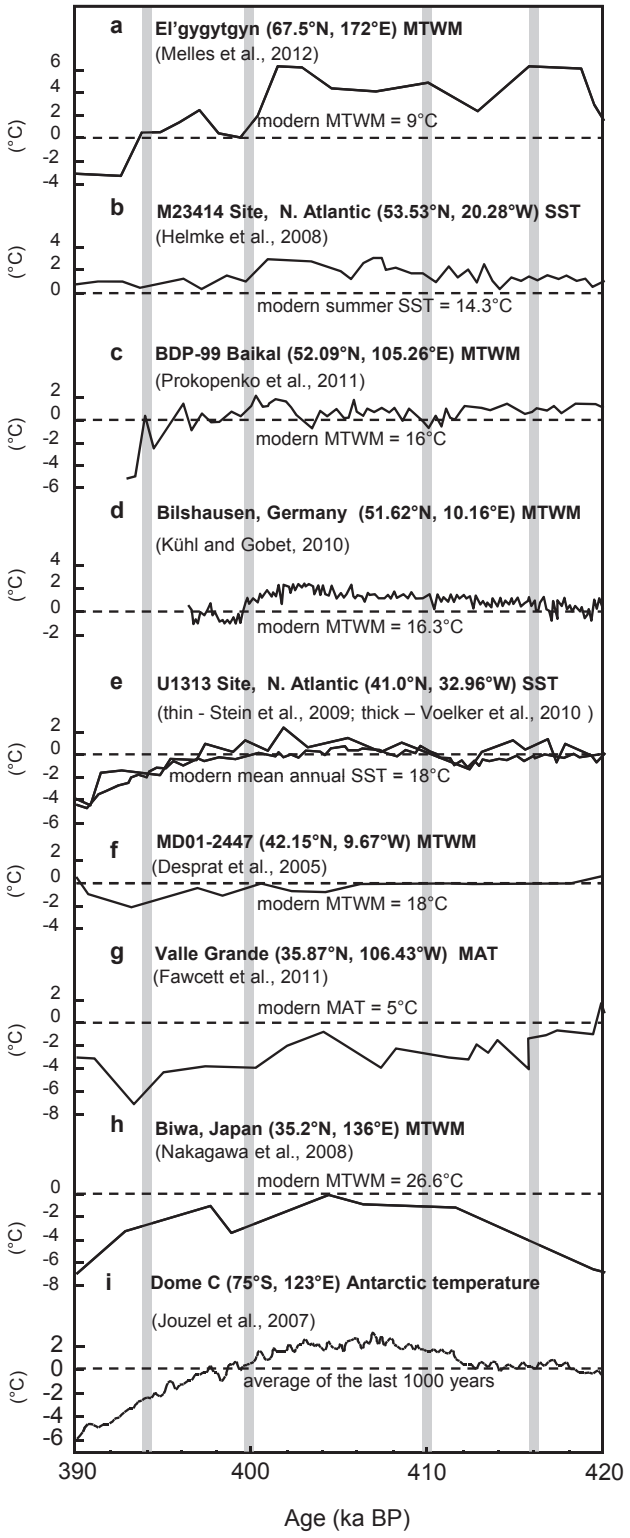

Fig. 9. Proxy-based reconstructions of temperature change between 420 and 390 ka and the present plotted against their respective time scales discussed in the cited publications. Grey bars mark the four time-slices analyzed by CLIMBER2-LPJ and CCSM3. Dashed line indicates the modern value.

(Stein et al., 2009) and M23414 (53.53°N, 20.28°W, Fig. 9b) (Helmke et al., 2008 modified from Kandiano and Bauch, 2007) in the northern Atlantic, suggesting that the mid-latitudes of Eurasia might have experienced less pronounced warming compared to the high Arctic regions, as was the case during the last interglacial (e.g. Velichko et al., 2008; Miller et al., 2010). The model simulations support this scenario, particularly by simulating warmer than present winters in the Arctic region but colder than present winters in mid-latitude Eurasia at 416 and 410 ka, in line with the pollen-based reconstruction of the mean temperature of the coldest month (MTCM) (Prokopenko et al., 2010).

Unlike the records from the northern high and mid- latitudes of continental Asia, the pollen-based climate reconstruction from Lake Biwa (35.2°N, 136°E) in central Japan (Nakagawa et al., 2008) demonstrates similar or even cooler than present summer temperatures between 420 and 390 ka (Fig. 9h), associated with relatively warm winters, which results in cooler than present mean annual temperatures (MAT) (Tarasov et al., 2011). Another reconstruction using a pollen record from Osaka Bay (Hongo, 2007) suggests that the interval between 414 and 398 ka experienced extremely warm winters (warm/subtropical climate), but attests the interval between 422 and 414 ka as one with relatively cool summer temperatures (Kariya et al., 2010). A MAT reconstruction comparable to that from Biwa was obtained using molecular palaeotemperature proxies in mid-Pleistocene lacustrine sediments from the Valles Caldera (35.87°N, 106.43°W), New Mexico (Fawcett et al., 2011), which also demonstrates that MAT values were 0–7 °C below the modern value of 5 °C during the interval under discussion (Fig. 9g). Wu et al. (2007), analyzing terrestrial mollusc assemblages in the Chinese Loess Plateau (~36° N, ~107–109°E), came to the conclusion that mean annual temperatures were warmer than present during the interval between 417 and 385 ka, with MAT values up to 2–4 °C above the modern. This conclusion is in line with earlier reconstructions based on pedological and geochemical properties of the MIS 11.3 sediment, suggesting that maximum values of MAT at Luochuan (35.75°N, 109.42°E) could be ~2–6 °C (Liu et al., 1985; Han et al., 1997; Guo et al., 1998) higher than the modern MAT. The models show warmer summers for the region at 416 and 410 ka, though winters are cooler, while the opposite holds for 400 ka.

In southern Europe the core MD01-2447 (42.15°N, 9.67°W), sediment retrieved ca. 100 km off the Iberian coast, has been used for a pollen-based climate reconstruction (Desprat et al., 2005). As in the northern lower latitudes of Asia, the reconstruction from the core MD01-2447 does not indicate climate warmer than at present, showing both summer and winter temperatures similar to or below present-day values for the entire MIS 11.3 timeframe, with temperatures cooling after 400 ka (Fig. 9f). Comparison with other climate archives from northern and central Europe is complicated by dating problems caused by discontinuities in the records. A lacustrine sediment core from La Côte (45.08°N, 5.57°E, 981 m) in the western French Alps was assigned to MIS 11 (Field et al., 2000). Coleoptera- and pollen-based climate reconstructions suggest conditions similar to present or even slightly warmer during the interglacial optimum, up to 18 °C in July compared to the modern value of 16.4 °C. However, pollen-derived mean January temperatures did not exceed the modern value (−0.7 °C) by more than ca. 1 °C, with the exception of one pollen spectrum (Field et al., 2000).

Koutsodendris et al. (2010) provided a high-resolution vegetation record from Dethlingen (52.96°N, 10.14°E) in northern Germany, which they assigned to the Holsteinian interglacial and correlated with MIS 11.3. However, neither absolute age control nor quantitative climate reconstructions are provided. Qualitative interpretation of the record suggests increasing warmth and temperate climate during the second half of MIS 11.3 (i.e. between 410 and 400 ka), in line with the available records from Antarctica and eastern Asia. Another supposedly MIS 11.3 record from the laminated sediment section at Bilshausen (51.62°N, 10.16°E, 160 m) in northern Germany provides a detailed pollen record and

quantitative reconstructions of mean July and mean January temperatures (Kühl and Gobet, 2010). The Bilshausen palaeoclimate record clearly shows that the warmest winter and summer temperatures occurred during the second half of the interglacial sequence, in line with the Dethlingen record. The reconstructions also demonstrate (Fig. 9d) that July temperatures were 1–2 °C higher than the modern value of 16.3 °C. During the interglacial optimum, reconstructed mean January temperature remained close to the modern values in the region (i.e. −0.7 °C); however, numerous colder oscillations (up to 2 °C below the present) appear in the reconstruction, suggesting some climate instability during this long interglacial interval. This reconstruction contradicts the qualitative reconstruction of MIS 11.3 climate obtained from the Ossowka pollen record (52.12°N, 23.13°E) in eastern Poland (Nitychoruk et al., 2005). The latter study characterizes the optimum phase of the interglacial as warmer than present with a long vegetation period, and mild and short winters, suggesting increasing oceanic influence on the regional climate. Kühl and Litt (2007) provide a somewhat intermediate scenario based on quantitative reconstructions from the ca. 16 ka long Holsteinian pollen records at Gröbern-Schmerz and Hetendorf/Munster-Breloh in northern Germany, concluding that January and July temperatures within the interglacial phase were comparable to present day conditions within a few degrees variation (i.e., within the accuracy of the reconstruction method). Other terrestrial records from Europe are less conclusive when discussing temperature changes. For example, faunal indicators from an absolutely dated Palaeolithic site at West Stow (52.32°N, 0.64°E) in the UK (Preece et al., 2007) suggest the climate was perhaps warmer than at present. Candy et al. (2010), summarizing available published interglacial records from southern England, also suggest that summer temperatures there could be as warm or even 1–2 °C warmer than at present during MIS 11.3, the range of the reconstructed mean temperature of the coldest month (−10 to +6 °C) allows MTCM to vary between ~13 and 14 °C below and ~2–3 °C above present-day values. The model projections show European summers warmer than preindustrial for 416 ka and 410 ka, while cooler temperatures prevail at 400 ka in both models and at 394 ka in CCSM3.

In summary, the interval between 420 and 400 ka is characterized by generally warmer then present summer temperatures, particularly in the high and high-middle latitudes. The data from the low-middle latitudes demonstrates similar to or colder than present summer and/or annual temperatures. Both proxy-based reconstructions and model simulations provide support for the regional diversity of climate change during MIS 11.3, suggesting that greenhouse gases are not the only forcing phenomenon and that other factors, including seasonal insolation (Yin and Berger, 2010), various amplifying feedbacks and distant teleconnections (Melles et al., 2012), also play a significant role.

4.2. Precipitation changes

Earlier data syntheses characterize the MIS 11.3 interglacial as rather humid, with higher and/or seasonally more uniform precipitation (e.g. Kukla, 2003; Rousseau, 2003). However, continuous records of precipitation are rare. One of them, coming from Lake El'gygytgyn, demonstrates that mean annual precipitation (MAP) values were ~100 to ~350 mm higher than at present between 400 and 420 ka (Fig. 10a), and decreased abruptly to the present day value of ca. 270 mm soon after 400 ka (Melles et al., 2012). Further south, in the Lake Baikal region a pollen-based MAP reconstruction also shows wetter conditions than at present (Fig. 10b), with MAP values 50–150 mm above the modern value between 420 and 396 ka and ca. 100 mm below modern at 394 ka (Prokopenko et al., 2010). Molluscan assemblages and soil property records from the Chinese Loess Plateau suggest that a humid climate prevailed there from 417 to 385 ka (Wu et al., 2007). Palaeopedological and geochemical studies on the Chinese loess sequences from the Loess Plateau (Guo et al., 1998) reconstructed MAP values 200–300 mm higher than modern in response to a much stronger Asian summer monsoon. Other authors (Liu et al., 1995; Han et al., 1997; Vidic et al., 2003) agree about a generally wet climate, but the suggested increase in precipitation is less pronounced. The Biwa Lake pollen record (Tarasov et al., 2011) shows MAP values up to 500 mm higher than at present at ca. 410 ka, slightly higher than at present at 416 and 400 ka, and ca. 200 mm lower than present at 394 ka (Fig. 10c). Results of the MAP simulations in the eastern Asian region presented in this paper are inconclusive. CLIMBER2-LPJ shows slightly higher than present MAP values at 416 ka, the maximum increase in precipitation at 410 ka and a decrease at 400 ka. CCSM3 experiments show a decrease in precipitation in the eastern part of China at 416 ka and 410 ka and an increase at 400 and 394 ka. Trends around Japan partly are the opposite.

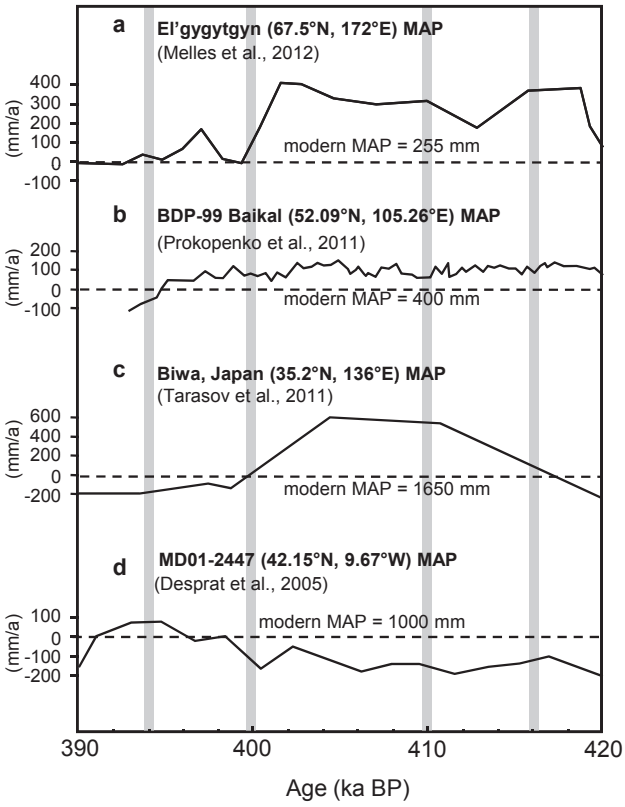

Fig. 10. Proxy-based reconstructions of mean annual precipitation change between 420 and 390 ka and the present plotted against their respective time scales discussed in the cited publications. Grey bars mark the four time-slices analyzed by CLIMBER2-LPJ and CCSM3. Dashed line indicates the modern value.

Proxy-based precipitation reconstructions from Europe demonstrate less pronounced changes in precipitation. Thus, coleopteran assemblages from La Côte in France suggest wetter conditions compared to the present during the interglacial optimum (Field et al., 2000). A pollen-based MAP reconstruction from the same site shows slightly higher or similar to present values. However, frequent oscillations towards drier than present climate are also reconstructed. The virtual absence of non-arboreal pollen (except Ericales) in the interglacial sediment from the site of Praclaux (44.82°N, 3.83°E; 1000 m) in the Massif Central, France, attributed to ca. 420–400 ka (Reille et al., 2000), can be used as

qualitative evidence of a wetter climate than during any subsequent interglacial. This interpretation of more humid conditions during MIS 11.3 correlates with the qualitative interpretation from the Ossowka, Poland, pollen record (Nitychoruk et al., 2005). A synthesis of the long continental records of MIS 11.3 (Rousseau, 2003) points (though not without reservations caused by the data and dating quality) to more humid than present climates in central Europe, tropical W Africa, central Japan, NW South America, and SE Australia, but suggesting drier than present conditions and increased Saharan influence in Israel. Pollen-based reconstruction of the MAP from the core MD01-2447, west of the Iberian Peninsula, also demonstrates values ca. 100–200 mm lower than at present between 416 and 400 ka at ca. 42°N latitude (Fig. 10d), but MAP values higher than at present at 394 ka (Desprat et al., 2005).

In the Atlantic region, the CLIMBER2-LPJ simulations demonstrate lower than present MAP values in the Mediterranean and higher values in tropical Africa at 416, 410 and 394 ka. The CCSM3 experiments show rather patchy results in the tropics and no substantial differences from the present in the middle and high latitudes.

4.3. Vegetation changes

Pollen records attributed to MIS 11.3 summarized at the global scale reveal the major expansion of forests after the preceding glacial and a very long forest phase in comparison with the subsequent interglacial periods (Rousseau, 2003). Recently published data from the Arctic region supports this earlier interpretation. The record from Lake El'gygytgyn (Melles et al., 2012; Tarasov et al., 2013) demonstrates that the sum of boreal trees and shrubs reached ca. 70–90% of the total pollen sum during the whole period between 420 and 400 ka, and dropped significantly after that time. The predominance of arboreal pollen in the pollen assemblages, particularly the high contents of spruce, indicates a boreal evergreen (taiga) forest as the dominant biome in the area, where treeless arctic tundra vegetation grows at present. The decline of the taiga biome scores and predominance of the tundra communities in the regional vegetation first occurred after about 400 ka. In a marine sediment core off southwest Greenland (ODP site 646: 58.21°N, 48.37°W), concentrations of seed plant and spruce pollen also reached the highest values of the last one million years after ca. 420 ka, suggesting dense vegetation cover and boreal coniferous (i.e. taiga-like) forest over the ice-free southern part of Greenland during the warmest phase of MIS 11 (de Vernal and Hillaire-Marcel, 2008). Since the climate models we employed were not configured with dynamic ice sheets, an ice-free southern Greenland could not be investigated with the models. For the El'gygytgyn area, however, both climate models show enhanced tree cover in LPJ for 416 and 410 ka, more pronounced in CCSM3. BIOME4 shows (dwarf) shrub tundra as the preindustrial biome, which is replaced by shrub tundra and even taiga forest in some locations. Therefore an expansion of trees is supported, but the BIOME4 model results suggest that the afforestation implied by the reconstructions may have been rather localized. For 400 and 394 ka, BIOME4 shows dwarf shrub tundra as the main biome, while LPJ shows reductions in vegetation cover, the timing of the transition would therefore agree with the reconstructions.

In the more southern region of Siberia around Lake Baikal the MIS 11.3 interval is also marked by a predominance of arboreal (mainly coniferous) taxa in the pollen records, and the highest percentages of fir pollen lead to the reconstruction of a long-lasting "conifer optimum" and the spread of taiga across the Lake Baikal region (Shichi et al., 2009; Prokopenko et al., 2010). The abundance of fir in the pollen assemblages (ca. 4–10% between 420 and 400 ka compared to 0–2% during the Holocene) is indicative of a climate warmer and wetter than during MIS 1 (Prokopenko et al., 2010), MIS 5.5 (Tarasov et al., 2005) or any other post-MIS 11.3 interglacial (Shichi et al., 2009). The models show evergreen taiga forest as the biome for all time slices except 410 ka, where the models show a shift to temperate grassland. The LPJ model suggests slight increases in tree cover west of Lake Baikal for 416 and 410 ka, i.e. the few grid cells not covered by trees in the preindustrial control are covered by trees in the experiments, but an increased coverage by grasses is not simulated, contrary to BIOME4.

The biome reconstruction from the Lake Biwa pollen record covering the last ca. 430 ka (Miyoshi et al., 1999) suggests that temperate deciduous forest predominated in the region between 420 and 390 ka, replacing the cool mixed forest vegetation which characterized the previous colder interval (Tarasov et al., 2011). Warm mixed forest (similar to the present day natural vegetation) is reconstructed during the warmest phase between ca. 410 and 400 ka, based on the presence of warm-temperate evergreen broadleaved trees such as *Quercus* subgenus *Cyclobalanopsis* and *Castanopsis*, which are less abundant during the more recent interglacial intervals (Miyoshi et al., 1999). The biome reconstruction results therefore demonstrate a similarity between the MIS 11.3 and the Holocene climatic optima in central Japan, which could reflect the warm winter temperatures required for evergreen broadleaved forest taxa to prosper (Prentice et al., 1992). The models do not support a shift from temperate deciduous to warm mixed forest, instead showing warm mixed forest for all time slices in BIOME4 and no change in tree coverage in LPJ.

Quantitative biome reconstructions from European pollen records of MIS 11.3 are limited. Temperate deciduous and cool mixed forest biomes are reconstructed as dominant vegetation types at La Côte in the western French Alps during the interglacial optimum (Field et al., 2000), while the taiga biome shows maximum scores at the beginning and at the end of the interglacial vegetation succession. The occurrence of *Pterocarya* (wingnut) and the highest percentages of fir pollen in European pollen records (e.g. Benda and Brandes, 1974; Nitychoruk et al., 2005; Diehl and Sirocko, 2007; Urban, 2007; Koutsodendris et al., 2010) has frequently been used as evidence of a wet climate, although interpretation of these pollen taxa in terms of temperature is ambiguous. The highest percentages of arboreal pollen in the MIS 11.3 interglacial records from France (Reille et al., 2000) also indicate greater tree coverage of the landscape in central Europe during the MIS 11.3 climatic optimum compared to any subsequent interglacial interval. For Europe, both models show warm mixed forest as the dominant biome north of the Iberian Peninsula for all time slices including preindustrial, and temperate woodland as the biome of the Iberian Peninsula and the Mediterranean region, while LPJ shows similar tree coverage to preindustrial. For 410 ka, the boundary between forest and woodland is shifted northwards into central France in the CLIMBER2-LPJ model, due to a decrease in precipitation in this particular grid cell. Models and vegetation reconstructions therefore agree in most cases, though the precipitation decrease in the CLIMBER2-LPJ model would not appear to be compatible with the reconstructions.

4.4. Synthesis

Summarizing the records listed above and in Figs. 9 and 10, the following picture emerges for the climate during MIS 11.3: Early during MIS 11.3, at 416 ka, JJA conditions were warmer than at present in the high northern latitudes at lakes Baikal and El'gygytgyn, while conditions in Japan were cooler. Europe and Antarctica show similar conditions to preindustrial. These qualitative trends are shown as grey circles in Fig. 2a, with light grey circles implying decreasing temperatures, white circles no change, and

dark grey circles increases in temperature. Precipitation was stronger than preindustrial at the Asian sites, and weaker than preindustrial in Europe, shown in Fig. 5a. Both models show substantially warmer conditions for Eurasia north of 40°N, so there is a disagreement between the models and the European records. For Japan, CCSM3 simulates much less warming than CLIMBER2-LPJ, more in line with the climate reconstruction. Precipitation trends in CLIMBER2-LPJ are similar to the reconstructions, but CCSM3 shows some discrepancies in locations where results are significant.

At the precession minimum at 410 ka, summer conditions were similar to or warmer than preindustrial in northern Siberia, Europe and Antarctica, while Japan remained cooler (Fig. 2b). The precipitation trends are similar to 416 ka (Fig. 5b). Both models show warmer temperatures for Eurasia with the exception of the monsoon regions. The JJA temperature reconstruction for Japan therefore is at odds with model results. Modelled precipitation changes seem to agree for CLIMBER2-LPJ, though CCSM3 shows trends opposite to the reconstructions, if signals are significant at all.

The precession maximum at 400 ka shows a warming in central Europe and central Asia, while the other sites show no temperature change or a cooling. The models generally show a cooling of JJA temperatures, therefore disagreeing with reconstructions for central Europe and Asia. The reconstructions show precipitation increases for central and northern Asia, with precipitation decreasing in Europe and not changing in Japan (Fig. 5c). The models show a small decrease in annual precipitation.

For 394 ka, finally, the reconstructions show no temperature change or a decrease (Fig. 2d), while they project a small warming for the Iberian peninsula but decreases or very little change for all other areas. For precipitation, finally, reconstructions (Fig. 5d) show decreases or no change, with the exception if the Iberian Peninsula, where an increase is reconstructed. The models agree overall, though an increase in Europe is not simulated.

5. Conclusions and outlook

The model simulations and proxy-based reconstructions summarized in this study agree that MIS 11.3 was a long lasting interglacial with conditions generally warmer than preindustrial, at least before 400 ka.

Both models used in this study support a northward expansion of trees at the expense of grasses in the high northern latitudes early during MIS 11.3, at 416 and 410 ka, especially in northern Asia and North America, in line with the available pollen-based reconstructions. According to the model results, these vegetation changes were driven by increased summer temperatures and, in some locations, increased annual rainfall. Again, higher than present annual precipitation values are also supported by the proxy records from central Europe, Siberia, China, and Japan. The modeled changes in temperature generally are confirmed by the reconstructions, which is not always the case for the modeled changes in annual precipitation. The rather large changes in annual precipitation reconstructed for some locations, especially the 30% increase in precipitation for Lake Biwa in Japan at 410 ka, are not supported by the model results.

Comparing the two climate models, the general patterns of simulated climate and vegetation changes appear rather similar, despite the substantially different resolutions of the two models. The general patterns are captured quite well by the low-resolution CLIMBER2-LPJ model, though the higher resolution of CCSM3 improves the representation of climate change in some areas like the monsoon regions. Temperature changes in the continental interiors seem to be underestimated by CLIMBER2-LPJ, especially during the time slices with decreases in radiative forcing in DJF at 416 ka and 410 ka and during JJA at 400 ka and 394 ka. Here, CCSM3 simulates lower temperatures than CLIMBER2-LPJ, especially over the continents, implying a higher sensitivity to insolation changes.

From the model simulations, it becomes very obvious that there was no single climate state during MIS 11.3, but rather a continuum of climate states, with JJA temperatures in Europe, for example, ranging from $\sim$2 °C colder than preindustrial to $\sim$3 °C warmer. Depending on orbital configuration and location investigated, climates warmer and colder, wetter and drier than preindustrial may all have occurred during this interglacial. Therefore, climate reconstructions without high dating quality are of very limited use in a model comparison and for investigating climate responses to external forcing. A climate reconstruction just claiming a date "some time during MIS 11" could represent any climate state during this long interglacial, and our model results make abundantly clear that there was a wide variety of possible climate states. Therefore high precision dating is essential, or else reconstructions cannot be compared to models that specify timing precisely.

From a modeling point of view, the wide range of climate states during MIS 11.3 to first order represents the response of the climate system to changes in insolation according to the orbital parameters. Therefore, climate changes have a latitudinal pattern, and deviations from this general pattern require local feedbacks to enhance the climate system response. In our model simulations, we show these feedbacks for the high latitudes, as well as the monsoon regions.

Overall, we successfully compared model results and climate/vegetation reconstructions for MIS 11. With respect to temperature, models and reconstructions tend to agree, though this is more ambivalent for precipitation. Our original aim had been to compare reconstructions and models at finer scales, but the scarcity of high-resolution well-dated records, as well as the coarse resolution of the models, prevented this. Both advanced models and a synthesis of accurately dated interglacial records therefore are necessary to understand the effects of the global-scale climate forcing on regional climate and vegetation.

Looking to future investigations, the lack of an ice sheet model is a clear shortcoming of the current model experiments. Since some reconstructions claim higher sea levels than preindustrial (Raymo and Mitrovica, 2012) and possibly a vegetated southern Greenland (de Vernal and Hillaire-Marcel, 2008), an investigation whether these conditions can actually be modelled under MIS 11.3 boundary conditions appears worthwhile. With regard to reconstructions, this paper has shown along with Yin and Berger (2012) and Herold et al. (2012) that climate changes in the Arctic and the monsoon areas may follow different patterns than climate changes in other areas. Therefore climate reconstructions using data from a single site do not allow any global conclusions. Instead, reconstructions need to rely on information from more than single sites in order to be reliable.

Acknowledgements

This paper is a contribution to the German Science Foundation (DFG) Priority Programme 1266 'Integrated Analysis of Interglacial Climate Dynamics (INTERDYNAMIC)'. Research of T. Kleinen, S. Hildebrandt and R. Rachmayani was financed via the DFG project 'Comparison of climate and carbon cycle dynamics during late Quaternary interglacials using a spectrum of climate system models, ice-core and terrestrial archives (COIN)'. S. Müller was financed via the DFG project 'Quantitative reconstructions of late Quaternary vegetation, temperature and atmospheric precipitation variability in eastern Siberia: Evaluation of ecosystem stability/instability during episodes of rapid climate change' (MU3181/1-1). The CCSM3 climate model experiments were run on the SGI Altix

Supercomputer of the "Norddeutscher Verbund für Hoch- und Höchstleistungsrechnen" (HLRN). P. Tarasov acknowledges the DFG Heisenberg program. Anne Dallmeyer kindly commented on an earlier version of this manuscript, leading to substantial improvement. We also thank two anonymous reviewers for their very constructive comments which helped to improve the manuscript substantially.

References

Ashton, N., Lewis, S.G., Parfitt, S.A., Penkman, K.E.H., Coope, G.R., 2008. New evidence for complex climate change in MIS 11 from Hoxne, Suffolk, UK. Quaternary Science Reviews 27, 652–668.

Bartlein, P.J., Harrison, S.P., Brewer, S., Conner, S., Davis, B.A.S., Gajewski, K., Guiot, J., Harrisson-Prentice, T.I., Henderson, A., Peyron, O., Prentice, I.C., Scholze, M., Seppä, H., Shuman, B., Sugita, S., Thompson, R.S., Viau, A.E., Williams, J., Wu, H., 2011. Pollen-based continental climate reconstructions at 6 and 21 ka: a global synthesis. Climate of the Past 37, 775–802.

Benda, L., Brandes, H., 1974. Die Kieselgur-Lagerstätten Niedersachsens, I: Verbreitung, Alter, Genese. Geologische Jahrbuch A 21, 3–85 (in German).

Berger, A., 1978. Long-term variations of daily insolation and Quaternary climatic changes. Journal of Atmospheric Sciences 35 (12), 2362–2367.

Berger, A., Loutre, M.F., 1991. Insolation values for the climate of the last 10 million years. Quaternary Science Reviews 10, 297–317.

Berger, A., Loutre, M.F., 1996. Modeling the climate response to the astronomical and CO_2 forcings. Comptes Rendues Academie des Sciences Paris 323 (II.a), 1–16.

Braconnot, P., Otto-Bliesner, B., Harrison, S., Joussaume, S., Peterchmitt, J.-Y., Abe-Ouchi, A., Crucifix, M., Driesschaert, E., Fichefet, T., Hewitt, C.D., Kageyama, M., Kitoh, A., Laîné, A., Loutre, M.-F., Marti, O., Merkel, U., Ramstein, G., Valdes, P., Weber, S.L., Yu, Y., Zhao, Y., 2007. Results of PMIP2 coupled simulations of the Mid-Holocene and Last Glacial Maximum – part 1: experiments and large-scale features. Climate of the Past 3, 261–277.

Brigham-Grette, J., Melles, M., Minyuk, P., Andreev, A., Tarasov, P., DeConto, R., Koenig, S., Nowaczyk, N., Wennrich, V., Rosén, P., Haltia-Hovi, E., Cook, T., Gebhardt, C., Meyer-Jacob, C., Snyder, J., Herzschuh, U., 2013. Pliocene warmth, polar amplification, and stepped Pleistocene cooling recorded in NE Arctic Russia. Science 340, 1421–1427.

Brovkin, V., Bendtsen, J., Claussen, M., Ganopolski, A., Kubatzki, C., Petoukhov, V., Andreev, A., 2002. Carbon cycle, vegetation, and climate dynamics in the Holocene: experiments with the CLIMBER-2 model. Global Biogeochemical Cycles 16 (4), 1139.

Brovkin, V., Ganopolski, A., Archer, D., Rahmstorf, S., 2007. Lowering of glacial atmospheric CO_2 in response to changes in oceanic circulation and marine biogeochemistry. Paleoceanography 22, PA4202. http://dx.doi.org/10.1029/2006PA001380.

Burckle, L.H., 1993. Late Quaternary interglacial stages warmer than present. Quaternary Science Reviews 12, 825–831.

Candy, I., Coope, G.R., Lee, J.R., Parfitt, S.A., Preece, R.C., Rose, J., Schreve, D.C., 2010. Pronounced warmth during the early Middle Pleistocene interglacials: investigating the Mid-Brunhes Event in the British terrestrial sequence. Earth-Science Reviews 103, 183–196.

Collins, W.D., Bitz, C.M., Blackmon, M.L., Bonan, G.B., Bretherton, C.S., Carton, J.A., Chang, P., Doney, S.C., Hack, J.J., Henderson, T.B., Kiehl, J.T., Large, W.G., McKenna, D.S., Santer, B.D., Smith, R.D., 2006. The Community Climate System Model Version 3 (CCSM3). Journal of Climate 19, 2122–2143.

Desprat, S., Sánchez Goñi, M.F., Turon, J.-L., McManus, J.F., Loutre, M.F., Duprat, J., Malaizé, B., Peyron, O., Peypouquet, J.-P., 2005. Is vegetation responsible for glacial inception during periods of muted insolation changes? Quaternary Science Reviews 24, 1361–1374.

de Vernal, A., Hillaire-Marcel, C., 2008. Natural variability of Greenland climate, vegetation, and ice volume during the past million years. Science 320, 1622–1625.

Diehl, M., Sirocko, F., 2007. A new Holsteinian pollen record from the dry maar at Döttingen (Eifel). In: Sirocko, F., Claussen, M., Sánchez Goñi, M.F., Litt, T. (Eds.), The Climate of the Past Interglacials, Development in Quaternary Science, vol. 7. Elsevier, Amsterdam, pp. 397–416.

Droxler, A.W., Farrell, J.W., 2000. Marine Isotope Stage 11(MIS 11): new insights for a warm future. Global Planetary Change 24 (1), 1–5.

Droxler, A.W., Poore, R., Burckle, L., 1999. Data on past climate warmth may lead to better model of warm future. Eos 80 (26), 289–290.

Droxler, A.W., Poore, R.Z., Burckle, L.H., 2003. Earth's Climate and Orbital Eccentricity – the Marine Isotope Stage 11 Question. In: Geophysical Monograph 137. American Geophysical Union, Washington DC.

Fawcett, P.J., Werne, J.P., Anderson, R.S., Heikoop, J.M., Brown, E.T., Berke, M.A., Smith, S.J., Goff, F., Donohoo-Hurley, L., Cisneros-Dozal, L.M., Schouten, S., Sinninghe Damsté, J.S., Huang, Y., Toney, J., Fessenden, J., WoldeGabriel, G., Atudorei, V., Geissman, J.W., Allen, C.D., 2011. Extended megadroughts in the southwestern United States during Pleistocene interglacials. Nature 470, 518–521. http://dx.doi.org/10.1038/nature09839.

Field, M.H., de Beaulieu, J.-L., Guiot, J., Ponel, P., 2000. Middle Pleistocene deposits at La Côte, Val-de-Lans, Isère department, France: plant macrofossil, palynological and fossil insect investigations. Palaeogeography, Palaeoclimatology, Palaeoecology 159, 53–83.

Ganopolski, A., Rahmstorf, S., Petoukhov, V., Claussen, M., 1998. Simulation of modern and glacial climates with a coupled global model of intermediate complexity. Nature 391, 351–356.

Ganopolski, A., Petoukhov, V., Rahmstorf, S., Brovkin, V., Claussen, M., Eliseev, A., Kubatzki, C., 2001. CLIMBER-2: a climate system model of intermediate complexity. Part II: model sensitivity. Climate Dynamics 17, 735–751.

Gerten, D., Schaphoff, S., Haberlandt, U., Lucht, W., Sitch, S., 2004. Terrestrial vegetation and water balance – hydrological evaluation of a dynamic global vegetation model. Journal of Hydrology 286, 249–270.

Guo, Z., Liu, T., Fedoroff, N., Wei, L., Ding, Z., Wu, N., Lu, H., Jiang, W., An, Z., 1998. Climate extremes in Loess of China coupled with the strength of deep-water formation in the North Atlantic. Global Planetary Change 18, 113–128.

Han, J., Keppens, E., Tungsheng, L., Paepe, R., Wenying, J., 1997. Stable isotope composition of the carbonate concretion in loess and climate change. Quaternary International 37, 37–43.

Haxeltine, A., Prentice, C.I., 1996. An equilibrium terrestrial biosphere model based on ecophysiological constraints, resource availability and competition among plant functional types. Global Biochemical Cycles 10 (4), 693–709.

Helmke, J.P., Bach, H.A., Röhl, U., Kandiano, E.S., 2008. Uniform climate development between the subtropical and subpolar Northeast Atlantic across marine isotope stage 11. Climate of the Past 4, 181–190.

Herold, N., Yin, Q.Z., Karami, M.P., Berger, A., 2012. Modelling the climatic diversity of the warm interglacials. Quaternary Science Reviews 56, 126–141.

Hodell, D.A., Charles, C.D., Ninnemann, U.S., 2000. Comparison of interglacial stages in the South Atlantic sector of the southern ocean for the past 450 kyr: implications for Marine Isotope Stage (MIS) 11. Global Planetary Change 24, 7–26.

Hongo, M., 2007. Stratigraphic distribution of *Hemiptelea* (Ulmaceae) pollen from Pleistocene sediments in the Osaka sedimentary basin, southwest Japan. Review of Palaeobotany and Palynology 144, 278–299.

Howard, W.R., 1997. A warm future in the past. Nature 388, 418–419.

Jolly, D., Haxeltine, A., 1997. Effect of low glacial atmospheric CO_2 on tropical African montane vegetation. Science 276, 786–788.

Jouzel, J., Masson-Delmotte, V., Cattani, O., Dreyfus, G., Falourd, S., Hoffmann, G., Minster, B., Nouet, J., Barnola, J.M., Chappellaz, J., Fischer, H., Gallet, J.C., Johnsen, S., Leuenberger, M., Loulergue, L., Luethi, D., Oerter, H., Parrenin, F., Raisbeck, G., Raynaud, D., Schilt, A., Schwander, J., Selmo, E., Souchez, R., Spahni, R., Stauffer, B., Steffensen, J.P., Stenni, B., Stocker, T.F., Tison, J.L., Werner, M., Wolff, E.W., 2007. Orbital and millennial Antarctic climate variability over the past 800.000 years. Science 317, 793–796.

Kandiano, E.S., Bauch, H.A., 2007. Phase relationship and surface water mass change in the Northeast Atlantic during Marine Isotope Stage 11 (MIS 11). Quaternary Research 68, 445–455.

Kaplan, J.O., 2001. Geophysical Applications of Vegetation Modeling (Ph.D. thesis). University of Lund.

Kaplan, J.O., New, M., 2006. Arctic climate change with a 2 °C global warming: timing, climate patterns and vegetation changes. Climate Change 79, 213–241.

Kaplan, J.O., Folberth, G., Hauglustaine, D.A., 2006. Role of methane and biogenic volatile organic compound scources in late glacial and Holocene fluctuations of atmospheric methane concentrations. Global Biogeochemical Cycles 20, GB2016. http://dx.doi.org/10.1029/2005GB002590.

Kariya, C., Hyodo, M., Tanigawa, K., Sato, H., 2010. Sea-level variation during MIS 11 constrained by stepwise Osaka Bay extensions and its relation with climatic evolution. Quaternary Science Reviews 29, 1863–1879.

Kleinen, T., Brovkin, V., von Bloh, W., Archer, D., Munhoven, G., 2010. Holocene carbon cycle dynamics. Geophysical Research Letters 37 (2), L02705. http://dx.doi.org/10.1029/2009GL041391.

Kleinen, T., Tarasov, P., Brovkin, V., Andreev, A., Stebich, M., 2011. Comparison of modeled and reconstructed changes in forest cover through the past 8000 years: Eurasian perspective. Holocene 5, 723–734. http://dx.doi.org/10.1177/0959683610386980.

Koutsodendris, A., Müller, U.C., Pross, J., Brauer, A., Kotthoff, U., Lotter, A.F., 2010. Vegetation dynamics and climate variability during the Holsteinian interglacial based on a pollen record from Dethlingen (northern Germany). Quaternary Science Reviews 29, 3298–3307. http://dx.doi.org/10.1016/j.quascirev.2010.07.024.

Kühl, N., Gobet, E., 2010. Climatic evolution during the Middle Pleistocene warm period of Bilshausen, Germany, compared to the Holocene. Quaternary Science Reviews 29, 3736–3749.

Kühl, N., Litt, T., 2007. Quantitative time-series reconstructions of Holsteinian and Eemian temperatures using botanical data. In: Sirocko, F., Claussen, M., Sánchez Goñi, M.F., Litt, T. (Eds.), The Climate of the Past Interglacials, Development in Quaternary Science, vol. 7. Elsevier, Amsterdam, pp. 239–254.

Kukla, G., 2003. Continental records of MIS 11. In: Droxler, A., Poore, R., Burckle, L. (Eds.), Earth's Climate and Orbital Eccentricity: The Marine Isotope Stage 11, Geophysical Monograph 137. American Geophysical Union, Washington DC, pp. 207–211.

Liesicki, E., Raymo, M.E., 2005. A Pliocene-Pleistocene stack of 57 globally distributed benthic $\delta^{18}O$ records. Paleoceanography 20. http://dx.doi.org/10.1029/2004PA001071.

Litt, T., Schölzel, C., Kühl, N., Brauer, A., 2009. Vegetation and climate history in the Westeifel Volcanic Field (Germany) during the last 11,000 years based on annually laminated lacustrine sediments. Boreas 38, 679–690.

Liu, T.S., An, Z., Yuan, B., Han, Z., 1985. The loess-paleosol sequence in China and climatic history. Episodes 8 (1), 21–28.
Liu, T.S., Guo, Z.T., Liu, J.Q., Han, J.M., Ding, Z.L., Gu, Z.Y., Wu, N.Q., 1995. Variations of eastern Asian monsoon over the last 140,000 years. Bulletin Societe Geologique France 166, 221–229.
Loulergue, L., Schilt, A., Spahni, R., Masson-Delmotte, V., Blunier, T., Lemieux, B., Barnola, J.-M., Raynaud, D., Stocker, T.F., Chappellaz, J., 2008. Orbital and millennial-scale features of atmospheric CH_4 over the past 800,000 years. Nature 453, 383–386.
Loutre, M.F., Berger, A., 2003. Marine Isotope Stage 11 as an analogue for the present interglacial. Global and Planetary Change 36, 209–217.
Loutre, M.F., 2003. Clues from MIS 11 to predict the future climate – a modelling point of view. Earth Planetary Sciences Letters 212, 213–224.
Lüthi, D., Le Floch, M., Bereiter, B., Blunier, T., Barnola, J.-M., Siegenthaler, U., Raynaud, D., Jouzel, J., Fischer, H., Kawamura, K., Stocker, T.F., 2008. High-resolution carbon dioxide concentration record 650.00-800.00 years before present. Nature 453, 379–382. http://dx.doi.org/10.1038/nature06949.
McManus, J., Oppo, D., Cullen, J., Healey, S., 2003. Marine isotope stage 11 (MIS 11): analog for Holocene and future climate? In: Droxler, A.W., Poore, R.Z., Burckle, L.H. (Eds.), Earth's Climate and Orbital Eccentricity: the Marine Isotope Stage 11 Question Geophysical Monograph Series, vol. 137 AGU, Washington, D.C., pp. 69–85.
McManus, J.F., Raynaud, D., Tzedakis, P.C., 2011. The 3rd PAGES Past Interglacials workshop. Pages News 19 (2), 80–81.
Melles, M., Brigham-Grette, J., Minyuk, P.S., Nowaczyk, N.R., Wennrich, V., DeConto, R.M., Anderson, P.M., Andreev, A.A., Coletti, A., Cook, T.L., Haltia-Hovi, E., Kukkonen, M., Lozhkin, A.V., Rosén, P., Tarasov, P., Vogel, H., Wagner, B., 2012. 2.8 Million years of Arctic climate change from Lake El'gygytgyn, NE Russia. Science 337, 315–320.
Merkel, U., Prange, M., Schulz, M., 2010. ENSO variability and teleconnections during glacial climates. Quaternary Science Reviews 29, 86–100.
Milker, Y., Rachmayani, R., Weinkauf, M.F.G., Prange, M., Raitzsch, M., Schulz, M., Kučera, M., 2013. Global and regional sea surface temperature trends during Marine Isotope Stage 11. Climate of the Past 9, 2231–2252. http://dx.doi.org/10.5194/cp-9-2231-2013.
Miller, G.H., Brigham-Grette, J., Alley, R.B., Anderson, L., Bauch, H.A., Douglas, M.S.V., Edwards, M.E., Elias, S.A., Finney, B.P., Fitzpatrick, J.J., Funder, S.V., Herbert, T.D., Hinzman, L.D., Kaufman, D.S., MacDonald, G.M., Polyak, L., Robock, A., Serreze, M.C., Smol, J.P., Spielhagen, R., White, J.W.C., Wolfe, A.P., Wolff, E.W., 2010. Temperature and precipitation history of the Arctic. Quaternary Science Reviews 29, 1679–1715.
Miyoshi, N., Fujiki, T., Morita, Y., 1999. Palynology of a 250-m core from Lake Biwa: a 430,000-year record of glacial-interglacial vegetation change in Japan. Review of Palaeobotany and Palynology 104, 267–283.
Nakagawa, T., Okuda, M., Yonenobu, H., Miyoshi, N., Fujiki, T., Gotanda, K., Tarasov, P.E., Morita, Y., Takemura, K., Horie, S., 2008. Regulation of the monsoon climate by two different orbital rhythms and forcing mechanisms. Geology 36, 491–494.
New, M., Hulme, M., Jones, P.D., 2000. Representing twentieth century space-time climate variability. Part 2: development of 1901-96 monthly grids of terrestrial surface climate. Journal of Climate 13, 2217–2238.
Nitychoruk, J., Bińka, K., Hoefs, J., Ruppert, H., Schneider, J., 2005. Climate reconstruction for the Holsteinian Interglacial in eastern Poland and its comparison with isotopic data from Marine Isotope Stage 11. Quaternary Science Reviews 24, 631–644.
Oleson, K.W., Niu, G.-Y., Yang, Z.-L., Lawrence, D.M., Thornton, P.E., Lawrence, P.J., Stöckli, R., Dickinson, R.E., Bonan, G.B., Levis, S., Dai, A., Qian, T., 2008. Improvements to the Community Land Model and their impact on the hydrological cycle. Journal of Geophysical Research 113, G01021. http://dx.doi.org/10.1029/2007JG000563.
Otto-Bliesner, B.L., Tomas, R., Brady, E.C., Ammann, C., Kothavala, Z., Clauzet, G., 2006. Climate sensitivity of moderate- and low-resolution versions of CCSM3 to preindustrial forcings. Journal of Climate 19, 2567–2583.
Petoukhov, V., Ganopolski, A., Brovkin, V., Claussen, M., Eliseev, A., Kubatzki, C., Rahmstorf, S., 2000. CLIMBER-2: a climate system model of intermediate complexity. Part I: model description and performance for present climate. Climate Dynamics 16, 1–17.
Preece, R.C., Parfitt, S.A., Bridgland, D.R., Lewis, S.G., Rowe, P.J., Atkinson, T.C., Candy, I., Debenham, N.C., Penkman, K.E.H., Rhodes, E.J., Schwenninger, J.-L., Griffiths, H.I., Whittaker, J.E., Gleed-Owen, C., 2007. Terrestrial environments during MIS 11: evidence from the Palaeolithic site at West Stow, Suffolk, UK. Quaternary Science Reviews 26, 1236–1300.
Prentice, I.C., Cramer, W., Hassison, S.P., Leemans, R., Monserud, R.A., Solomon, A.M., 1992. A global biome model based on plant physiology and dominance, soil properties and climate. Journal of Biogeography 19, 117–134.
Prokopenko, A.A., Hinnov, L.A., Williams, D.F., Kuzmin, M.I., 2006. Orbital forcing of continental climate during the Pleistocene: a complete astronomically tuned climatic record from Lake Baikal, SE Siberia. Quaternary Science Reviews 25, 3431–3457.
Prokopenko, A.A., Bezrukova, E.V., Khursevich, G.K., Solotchina, E.P., Kuzmin, M.I., Tarasov, P.E., 2010. Climate in continental interior Asia during the longest interglacial of the past 500 000 years: the new MIS 11 records from Lake Baikal, SE Siberia. Climate of the Past 6, 31–48.
Raymo, M.E., Mitrovica, J.X., 2012. Collapse of polar ice sheets during the stage 11 interglacial. Nature 483, 453–456.
Reille, M., de Beaulieu, J.-L., Svobodova, H., Andrieu-Ponel, V., Goeury, C., 2000. Pollen analytical biostratigraphy of the last five climatic cycles from a long continental sequence from the Velay region (Massif Central, France). Journal of Quaternary Science 15, 665–685.
Rousseau, D.-D., 2003. The continental record of stage 11: a review. In: Droxler, A., Poore, R., Burckle, L. (Eds.), Earth's Climate and Orbital Eccentricity: The Marine Isotope Stage 11 Question, Geophysical Monograph 137. American Geophysical Union, Washington DC, pp. 213–222.
Ruddiman, W.F., 2003. The Anthropogenic Greenhouse Era began thousands of years ago. Climatic Change 61, 261–293.
Schilt, A., Baumgartner, M., Blunier, T., Schwander, J., Spahni, R., Fischer, H., Stocker, T.F., 2010. Glacial-interglacial and millennial scale variations in the atmospheric nitrous oxide concentration during the last 800,000 Years. Quaternary Science Reviews 29, 182–192.
Shichi, K., Takahara, H., Kawamuro, K., 2009. Vegetation and climate changes during MIS 11 in southeastern Siberia based on pollen records from Lake Baikal sediment. Japan. Journal of Palynology 55, 3–14.
Siegenthaler, U., Stocker, T.F., Monnin, E., Lüthi, D., Schwander, J., Stauffer, B., Raynaud, D., Barnola, J.-M., Fischer, H., Masson-Delmotte, V., Jouzel, J., 2005. Stable carbon cycle-climate relationship during the Late Pleistocene. Science 310, 1313–1317.
Sitch, S., Smith, B., Prentice, I.C., Arneth, A., Bondeau, A., Cramer, W., Kaplan, J.O., Levis, S., Lucht, W., Sykes, M.T., Thonicke, K., Venevsky, S., 2003. Evaluation of ecosystem dynamics, plant geography and terrestrial carbon cycling in the LPJ dynamic global vegetation model. Global Change Biology 9, 161–185.
Solomon, S., Qin, D., Manning, M., Chen, Z., Marquis, M., Averyt, K.B., Tignor, M., Miller, H.L. (Eds.), 2007. Contribution of Working Group I to the Fourth Assessment Report of the Intergovernmental Panel on Climate Change. Cambridge University Press, Cambridge, United Kingdom and New York, NY, USA.
Stein, R., Hefter, J., Grützner, J., Voelker, A., Naafs, B.D.A., 2009. Variability of surface water characteristics and Heinrich-like events in the Pleistocene midlatitude North Atlantic Ocean: biomarker and XRD records from IODP Site U1313 (MIS 16–9). Paleoceanography 24, PA2203,. http://dx.doi.org/10.1029/2008PA001639.
Tarasov, P., Granoszewski, W., Bezrukova, E., Brewer, S., Nita, M., Abzaeva, A., Oberhänsli, H., 2005. Quantitative reconstruction of the last interglacial vegetation and climate based on the pollen record from Lake Baikal, Russia. Climate Dynamics 25, 625–637.
Tarasov, P.E., Bezrukova, E.V., Krivonogov, S.K., 2009. Late Glacial and Holocene changes in vegetation cover and climate in southern Siberia derived from a 15 kyr long pollen record from Lake Kotokel. Climate of the Past 5, 285–295.
Tarasov, P.E., Nakagawa, T., Demske, D., Österle, H., Igarashi, Y., Kitagawa, J., Mokhova, L., Bazarova, V., Okuda, M., Gotanda, K., Miyoshi, N., Fujiki, T., Takemura, K., Yonenobu, H., Fleck, A., 2011. Progress in reconstruction of Quaternary climate dynamics in the Northwest Pacific: a new modern-analogue reference dataset and its application to the 430-kyr pollen record from Lake Biwa. Earth-Science Reviews 108, 64–79.
Tarasov, P.E., Williams, J.W., Kaplan, J.O., Österle, H., Kuznetsova, T.V., Wagner, M., 2012. Environmental change in the temperate grasslands and steppe. In: Matthews, J.A., Bartlein, P.J., Briffa, K.R., Dawson, A.G., de Vernal, A., Denham, T., Fritz, S.C., Oldfield, F. (Eds.), The SAGE Handbook of Environmental Change, Human Impacts and Responses, vol. 2. SAGE Publications Ltd., Los Angeles, pp. 215–244.
Tarasov, P.E., Andreev, A.A., Anderson, P.M., Lozhkin, A.V., Leipe, C., Haltia, E., Nowaczyk, N.R., Wennrich, V., Brigham-Grette, J., Melles, M., 2013. 2013. A pollen-based biome reconstruction over the last 3.562 million years in the Far East Russian Arctic – new insights into climate–vegetation relationships at the regional scale. Climate of the Past 9, 2759–2775.
Tzedakis, P.C., Raynaud, D., McManus, J.F., Berger, A., Brovkin, V., Kiefer, T., 2009. Interglacial diversity. Nature Geoscience 2, 751–755. http://dx.doi.org/10.1038/NGEO0660.
Tzedakis, P.C., 2010. The MIS 11-MIS 1 analogy, southern European vegetation, atmospheric methane and the "early anthropogenic hypothesis". Climate of the Past 6, 131–144.
Urban, B., 2007. Interglacial pollen records from Schöningen, North Germany. In: Sirocko, F., Claussen, M., Sánchez Goñi, M.F., Litt, T. (Eds.), The Climate of the Past Interglacials, Development in Quaternary Science, vol. 7. Elsevier, Amsterdam, pp. 417–444.
Velichko, A.A., Borisova, O.K., Zelikson, E.M., 2008. Paradoxes of the Last Interglacial climate: reconstruction of the northern Eurasia climate based on palaeofloristic data. Boreas 37 (19), 1–19.
VEMAP Members, 1995. Vegetation/Ecosystem Modeling and Analysis Project (VEMAP): comparing biogeography and biogeochemistry models in a continental-scale study of terrestrial ecosystem responses to climate change and CO_2 doubling. Global Biogeochemical Cycles 9 (4), 407–437.
Vidic, N.J., Verosub, K.L., Singer, M.J., 2003. The Chinese Loess perspective on marine isotope Stage 11 as an extreme interglacial. In: Droxler, A.W., Poore, R.Z., Burckle, L.H. (Eds.), Earth's Climate and Orbital Eccentricity – the Marine Isotope Stage 11 Question, Geophysical Monograph 137. American Geophysical Union, Washington DC, pp. 231–240.
Voelker, A.H.L., Rodrigues, T., Billups, K., Oppo, D.W., McManus, J.F., Stein, R., Hefter, J., Grimalt, J.O., 2010. Variations in mid-latitude North Atlantic surface water properties during the mid-Brunhes (MIS 9-14) and their implications for the thermohaline circulation. Climate of the Past 6 (4), 531–552.
Wanner, H., Beer, J., Bütekofer, J., Crowley, T.J., Cubasch, U., Flückinger, J., Goosse, H., Grosjean, M., Joos, F., Kaplan, J.O., Küttel, M., Müller, S.A., Prentice, I.C.,

Solomina, O., Stocker, T.F., Tarasov, P., Wagner, M., Widmann, M., 2008. Mid- to Late Holocene climate change: an overview. Quaternary Science Reviews 27, 1791–1828.

Weber, A.W., Link, D.W., Schurr, T. (Eds.), 2010. Prehistoric Hunter-Gatherers of the Baikal Region, Siberia: Bioarchaeological Studies of Past Lifeways. University of Pennsylvania Museum of Archaeology and Anthropology, Philadelphia.

Wu, N., Chen, X., Rousseau, D.D., Li, F., Pei, Y., Wu, B., 2007. Climate conditions recorded by terrestrial mollusc assemblages in the Chinese Loess Plateau during marine Oxygen Isotope Stage 12-10. Quaternary Science Reviews 26, 1884–1896.

Yasuda, Y., Shinde, V. (Eds.), 2004. Monsoon and Civilization. Roli Books Pvt. Ltd., New Delhi.

Yeager, S.G., Shields, C.A., Large, W.G., Hack, J.J., 2006. The low-resolution CCSM3. Journal of Climate 19, 2545–2566.

Yin, Q.Z., Berger, A., 2010. Insolation and CO_2 contribution to the interglacial climate before and after the Mid-Brunhes Event. Nature Geoscience 3, 243–246. http://dx.doi.org/10.1038/NGEO0771.

Yin, Q.Z., Berger, A., 2012. Individual contribution of insolation and CO_2 to the interglacial climates of the past 800,000 years. Climate Dynamics 38, 709–724. http://dx.doi.org/10.1007/s00382-011-1013-5.